ETH
Eidgenössische Technische Hochschule Zürich
Swiss Federal Institute of Technology Zurich

eeh power systems laboratory

swissgrid

Andreas Ritter

Deterministic Sizing of the Frequency Bias Factor of Secondary Control

Semester Thesis
PSL1106

EEH – Power Systems Laboratory
Swiss Federal Institute of Technology (ETH) Zurich

In Cooperation with swissgrid ag

Expert: Prof. Dr. Göran Andersson
Supervisors: MSc ETH Marc Scherer,
MSc ETH Emil Iggland

Zurich, June 1, 2011

Abstract

An important challenge of grid control is the prediction of the frequency bias factor K_i so as to be as well matched to the actual frequency response characteristic β_i of an area i as possible, in order to adhere to the principle of non-interaction in Secondary Control. In this report, new semi-online sizing methods based on extensive previous research and on the current operation policies in Continental Europe are presented. Data directly from Switzerland's TSO swissgrid is analyzed and used as basis for an evaluation of the sizing methods in a purpose-designed simulation.

Contents

Chapter 1

Introduction

Maintaining the balance between mechanical power fed into all generators and the active power consumed by all loads is one of the most crucial control problems in a synchronous grid. In the former UCPTE and Union for the Co-ordination of Transmission of Electricity (UCTE)[1], a fast acting frequency-dependent Primary Control loop combined with a slower but error-free Secondary Control loop has been maintaining this balance for over 50 years. With the advent of liberalization, electricity trading and uncontrollable renewable energies, the fundamentals of the interconnection have changed beyond regular expansion to new countries, while the frequency control mechanisms remain in their original form.
This project focuses on the sizing of the frequency bias factor K_i, a fundamental component of Secondary Control, which has seen little change over the last decades.
To determine shortcomings of the currently implemented methods and to outline potential improvements, this project was completed at the request of Switzerland's Transmission System Operator (TSO) swissgrid ag in cooperation with the Power Systems Laboratory at ETH Zurich.

[1]Now referred to as the Regional Group Continental Europe (RGCE) of European Network of Transmission System Operators for Electricity (ENTSO-E).

Chapter 2

Frequency Control Theory

It is well established that a mismatch between mechanical energy fed into electric generators $P_m(t)$ and active electric power consumed by loads and losses $P_e(t)$ is balanced by reducing or increasing the energy stored in the rotating masses W_{rot} in the electric power system according to equation (2.1). From equation (2.2) it is clear that a change in the rotational energy can only result in a change of the system frequency f.

$$P_m(t) + \frac{dW_{rot}}{dt} - P_e(t, f) = 0 \quad \forall t \tag{2.1}$$

$$W_{rot} = \frac{1}{2} J (2\pi f)^2 \tag{2.2}$$

Detailed analyses of these dynamics can be found in [1] and [2]. The notation in this chapter will closely follow [2].

2.1 Need for Constant Frequency

Equipment, from home appliances to steam turbines, connected to a synchronous grid, is designed to operate at this grid's nominal frequency which is 50 Hz in Europe. Small deviations from the nominal frequency, in the range of a few millihertz, are a normal result of stochastic variations in loads and should not affect the behavior of any component in the network. Large deviations, in the range of one Hertz or above, however, carry a number of dangers and have to be avoided. Especially large electric motors and generators, whose rotational speed are directly proportional to the square of the electric frequency, are at risk from vibratory stress due to resonances. Another hazard stems from magnetic saturation in power transformers and induction motors [1].
According to the 2009 Union for the Co-ordination of Transmission of Electricity (UCTE) Operation Handbook (OpHB) [3], as a result of the "maximum instantaneous power deviation between generation and demand in the

un-split synchronous area, [...] undisturbed operation depends on the size of the synchronous area and the largest generation unit or generation capacity connected to a single bus bar"[1]. The frequency is allowed to deviate no more than 800 mHz in either direction immediately after the incident and no more than 200 mHz in the quasi-steady state following the disturbance. If the system frequency drops below 49 Hz, the 2004 UCTE OpHB recommends TSOs disconnect between 10 and 20 % of their loads (load shedding) and again 10 to 15 % more at the trigger frequencies 48.7 Hz and 48.4 Hz as emergency actions. Below frequencies of 47.5 Hz power plants are advised to disconnect immediately to avoid damage [4].

2.2 Without Speed Governing

In steady state, $P_m = P_e$ which results in a constant rotational energy and therefore constant mechanical and electrical frequencies. In an interconnected system, a sudden loss of electric power produced in one generator (i.a. resulting from a generator trip) is compensated by all other generators releasing energy stored as inertia of their rotating masses. Equation (2.2) shows that the frequency f will decrease with the square root of the rotational energy. This collapse of the system frequency is somewhat counteracted by the self-regulation effect of electric loads, leading to a reduced consumption of electrical power at decreased frequencies. As a result of this effect, a new steady state will be reached at a lower frequency. Self-regulation is the subject of numerous research efforts, for network modeling it is generally assumed that the load changes proportionally to the frequency according to equation (2.3)[2]. The load damping factor D_l as defined in equation (2.4), is generally found to be between 0%/Hz and 4%/Hz (0−2%/%) [2]; it is sometimes given directly in the unit of MW/Hz when referring to a defined network[3].

$$\Delta P_e = \boldsymbol{D_l} \cdot \Delta f \tag{2.3}$$

$$\boldsymbol{D_l} \left[\frac{\%}{\mathrm{Hz}}\right] = \frac{\frac{P_0 - P}{P_0}}{f_0 - f} \tag{2.4}$$

In order to illustrate this effect, the steady state frequency at which the Swiss network would settle if it were not interconnected with other networks and had no frequency control is calculated. Data from ENTSO-E's Statistical

[1] This "Reference Incident" is currently defined as 3000 MW in European Network of Transmission System Operators for Electricity (ENTSO-E).

[2] [2] features an additional term from rotating mass loads, which depends on $\frac{df}{dt}$. While it influences the time-characteristics of the decrease, it does not influence the resulting steady state frequency.

[3] In this report, bold $\boldsymbol{D_l}$ refers to values given in the relative unit of %/Hz and %/%, while regular D_l refers to load dampings in the unit of MW/Hz.

Yearbook 2009 [5] was used for an exemplary calculation. The highest measured load in Switzerland in 2009 was $P_{total} = 10261\,\mathrm{MW}$, the largest single producer in operation is the nuclear plant in Leibstadt with a generator rating of $P_{missing} = 1165\,\mathrm{MW}$. If the self-regulation effect of the load is assumed to be $D_l = 2\%/\mathrm{Hz}$, the frequency would settle at 44.3 Hz, 5.7 Hz below the nominal frequency of 50.0 Hz according to (2.5). This is clearly far below the tripping point of most power plants and thus unacceptable.

$$\frac{P_{missing}}{P_{total}} \cdot \frac{1}{\boldsymbol{D_l}} = f_0 - f = 11.4\,\% \cdot \frac{1}{2\frac{\%}{\mathrm{Hz}}} = 5.7\,\mathrm{Hz} \tag{2.5}$$

2.3 Three Tiered Approach

In most large interconnections, frequency control is split into three feedback loops which have distinct goals, time-scales and activation mechanisms. The differences in time-scales uncouples the three control loops so that they can be dimensioned and analyzed separately.
Figure 2.1 shows an interconnection consisting of three synchronously connected areas. Every area has multiple generators (G) and one load ($L1$-$L3$), representing the sum of all loads in the area. The tie-lines connecting the areas carry power between the areas according to a previously defined schedule. Figure 2.2 shows the cooperation of the three control loops in case of a generator failure in area 1, to restore pre-failure conditions according to ENTSO-E regulations. As explained previously, a lack of generation will lead to a frequency decrease. This decrease will be limited by the activation of Primary Control in all synchronously connected areas, which in turn changes the flow of tie-line power to help the area in need. Primary Control does not aim to restore the frequency to its pre-fault value but merely to dampen the system's dynamics and to settle the frequency at an acceptable quasi-steady state until it can be restored. It has to be fully available after 30 s and last for at least 15 min. Summed up over the whole synchronous area, the available Primary Control reserve is usually chosen to be as large as the biggest generation and load loss that can occur from one single fault (e.g. bus-bar failure, unprovoked load shedding). This assures that the frequency does not reach dangerous levels after a single outage. Multiple outages in short succession, however, can compromise the system's security, which is why the Primary Control has to be relieved shortly after the quasi-steady state frequency has been reached.
After a quasi-steady state frequency has been reached, the Secondary Control loop steps in to restore the tie-line power flows to pre-fault levels and to bring the frequency back to the nominal value, releasing the Primary Control reserves for further disturbances. Both Primary and Secondary Control

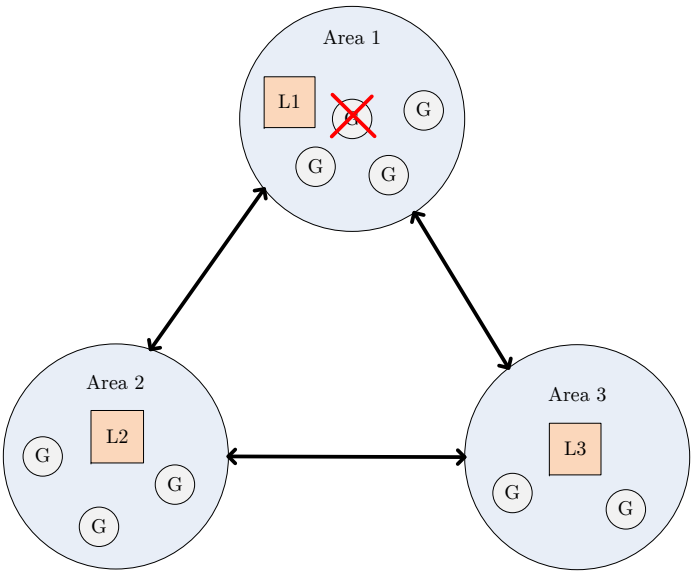

Figure 2.1: Three Area System with Tie-Lines and individual Loads (L1-3) and Generators (G).

are usually[4] applied automatically.
A third reserve, the so called Tertiary Control reserve, can be activated by an operator in the affected area to support Secondary Control and to release its resources until the missing generation or load can be balanced by changing the operation schedule of a regular (i.e. non-control) power plant. Secondary Control Reserves (oftentimes with the help of Tertiary) have to be able to replace the largest possible generation and load failure in their area as defined by the OpHB.

2.4 Primary Control Using Speed Droop Control

Primary Control is implemented by a simple proportional feedback loop between the electric frequency and the turbine governor. Equation (2.6) defines the speed droop "S", usually given in the unit of (% frequency deviation)/(100% power deviation) or simply %, of a generator or (Hz frequency deviation)/(MW power deviation) for a network of generators[5]. Speed droop is defined to be the relationship between system frequency deviation and resulting generator power output change and as such is used as proportionality

[4] In the Regional Group Continental Europe, all Primary and Secondary Control is activated and controlled automatically while some other interconnections choose to activate Secondary Control manually.

[5] As with the load damping factor D_l, bold $\boldsymbol{S}$ refers to relative speed droops in (% frequency)/(100% power), while regular S implies the more common unit of Hz/MW

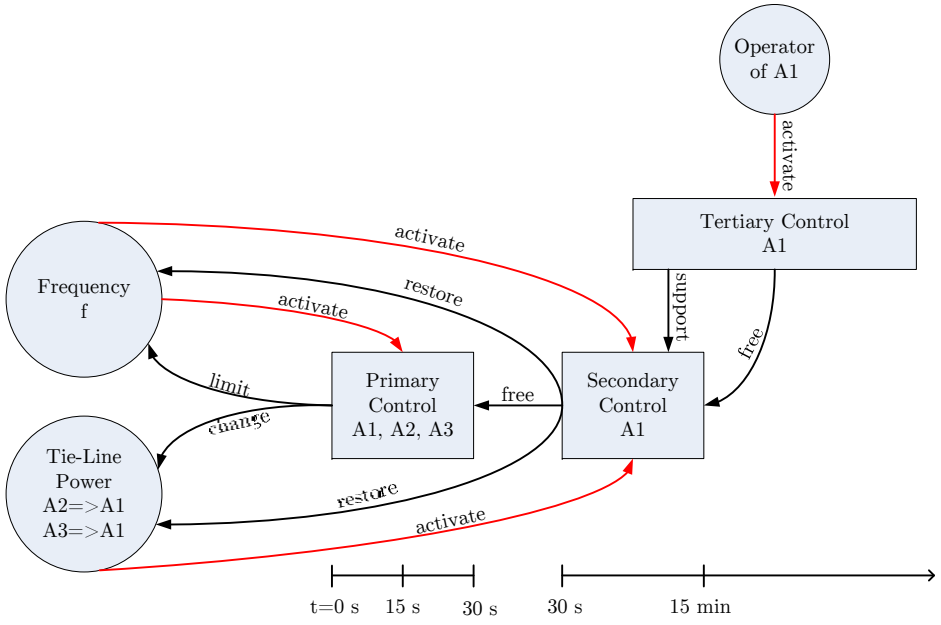

Figure 2.2: Interactions in Frequency Controls. Red Arrows: Control Inputs; Black Arrows: Effects of Control Actions.

constant in the control loop of turbine governors. It determines the generator's change in power output ΔP from its scheduled value P_{sched} for every frequency f as seen in figure 2.3 after the various turbine dynamics have decayed.

$$S = -\frac{\frac{\Delta f}{f_{Nom}}}{\frac{\Delta P}{P_{Gen}}} \tag{2.6}$$

If the frequency deviates too far from its nominal value however, Primary Control generators are required to fully activate their primary reserve regardless of their speed droop. This requirement introduces non-linear jumps, leaving only a certain frequency range for linear control as illustrated in figure 2.3. In the Regional Group Continental Europe (RGCE) this band extends ±200 mHz around the nominal frequency.
The simplicity of this mechanism assures that participating generators in all areas work together without competing, but it also leaves a steady state error, which has to be corrected by another control loop. As mentioned in section 2.2, in addition to the change in power produced by generators, the power consumed by the loads of a system also changes with its frequency. Equation (2.7) sums up these two effects for a change in load power of ΔP_{load}, resulting in the quasi-steady state frequency f_{ss} in equation (2.8) at which the interconnected network will settle after Primary Control has

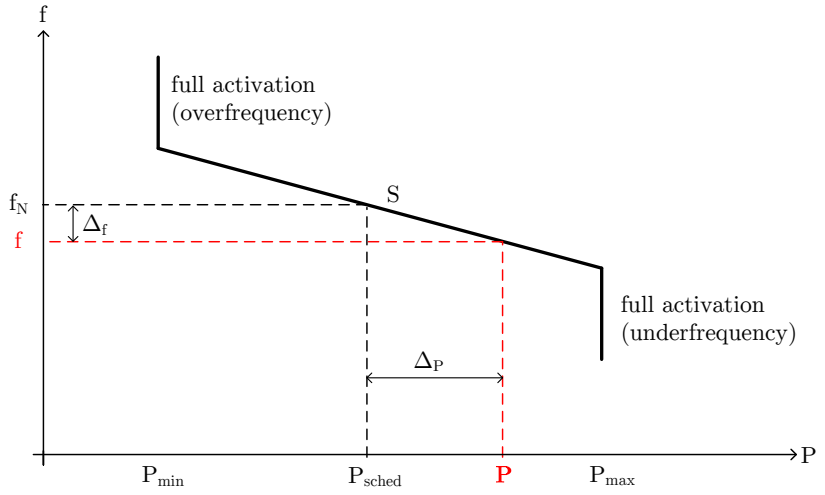

Figure 2.3: Linear Speed Droop Constant of a Generator with Underfrequency and Overfrequency Activation.

been fully deployed and the turbine dynamics have settled.

$$\Delta f_{ss} = -\Delta P_{load} \cdot \frac{1}{D_l + \frac{1}{S}} \tag{2.7}$$

$$f_{ss} = f_{Nom} + \Delta f_{ss} \tag{2.8}$$

In ENTSO-E's regional group Continental Europe, the total Primary Control reserve is set to the size of the reference incident, 3000 MW, and distributed over the control blocks roughly according to their share of the total power production in the interconnection. This distribution allows control blocks to be protected against large frequency deviations without having to reserve the full generation power they would need for their worst case scenarios.
Extending the example used in section 2.2, it is obvious that Switzerland, were it not interconnected, would need at least 1165 MW in Primary Control reserve to protect the grid frequency from an outage of its largest power plant, neglecting load self-regulation. This represents about 15.4 % of the average electric power production of Switzerland in 2009. For comparison, Switzerland's share of the 3000 MW Continental Europe reserve is currently 77 MW, a mere 1 % of the average power [6]. This is clearly an advantage over providing the full reserve for a worst-case scenario, as Primary Control reserves are expensive to maintain [7]. Applying equation (2.7), it can be calculated that an outage of the 1165 MW generator at Leibstadt would lead

to a frequency deviation of between -53 mHz and -64 mHz[6] in RGCE.

2.5 Frequency Response Characteristic

The sum of the effect of speed droop governing and of the self-regulation of loads determines the steady state frequency deviation after a disturbance, as shown in equation (2.7). This sum is called "frequency response characteristic" and usually labeled β[7]. Calculation for every area i is done according to equation (2.9).
Connecting areas synchronously provides the Primary Control power and the change in load from self-regulation available in all areas for an incident in any of the areas. Thus the individual frequency response characteristics β_i can be summed into one frequency response characteristic β for the whole interconnection as shown in equation (2.10) and equation (2.11). To compare the behavior of a network to that of a generator, the effective speed droop σ in [%frequency] of that network can be calculated according to equation (2.12).

$$\beta_i = \frac{1}{S_i} + D_{l,i} \tag{2.9}$$

$$-\Delta P_{load} = \Delta f_{ss} \cdot \sum_i (D_{l,i} + \frac{1}{S_i}) \tag{2.10}$$

$$\beta = \sum_i \beta_i \tag{2.11}$$

$$\sigma = \frac{1}{\beta} \cdot \frac{P_{total}}{f_N} \cdot 100\% \tag{2.12}$$

This provides an elegant way to write equation (2.7) for interconnected areas, equation (2.13).

$$\Delta f_{ss} = -\frac{\Delta P_{load}}{\beta} \tag{2.13}$$

That said, some caution has to be exercised when adding the speed droops and load damping factors of different machines and networks, because percentages can be calculated on different bases. Speed droops can easily be converted from $\boldsymbol{S}$ [%] to S [Hz/MW] according to equation (2.14) via division by the generator rating and multiplication by the nominal frequency. Once given in Hz/MW speed droops can simply be summed as shown to equation (2.15). To convert the sum of speed droops $S_{gen,tot}$ to $\boldsymbol{S_{gen,tot}}$ [%] it has to

[6] Calculated using 2 % self-regulation of the loads at the highest (405158 MW) and lowest (201878 MW) load measured in 2009 according to [5].

[7] The definition of β as $\Delta_{power}/\Delta_{frequency}$ in this report follows the notation of [1]. The UCTE OpHBs use the greek letter λ for the same definition. In some other literature, however, the network response characteristic is definded as network speed droop S or σ, being equivalent to $\frac{1}{\beta}$.

be multiplied by the combined ratings of the participating generators and divided by the nominal frequency as illustrated in equation (2.16).

$$S_{gen,i}\ \left[\tfrac{\text{Hz}}{\text{MW}}\right] = \boldsymbol{S_{gen,i}} \cdot \frac{f_N}{P_{gen,i}} \cdot \frac{1}{100} \tag{2.14}$$

$$S_{gen,tot}\ \left[\tfrac{\text{Hz}}{\text{MW}}\right] = \frac{1}{\sum_{i=1}^{N} \frac{1}{S_i}} \tag{2.15}$$

$$\boldsymbol{S_{gen,tot}}\ [\%] = S_{gen,tot} \cdot \frac{\sum_{i=1}^{N} P_{gen,i}}{f_N} \cdot 100\% \tag{2.16}$$

Analogously, the load damping factors $\boldsymbol{D_{l,i}}\,[\frac{\%}{\text{Hz}}]$ have to be multiplied by their load powers $P_{load,i}$ to be converted to $D_{l,i}\,[\frac{\text{MW}}{\text{Hz}}]$ in order to avoid unit mismatches. Equations (2.17) to (2.19) illustrate the necessary calculations. The conversion from $\boldsymbol{D_l}$ in $[\frac{\%}{\text{Hz}}]$ to $[\frac{\%}{\%}]$ is a simple division by two, as shown in equation (2.20).

$$D_{l,i}\ \left[\tfrac{\text{MW}}{\text{Hz}}\right] = \frac{1}{100}\boldsymbol{D_{l,i}} \cdot P_{load,i} \tag{2.17}$$

$$D_{l,tot}\ \left[\tfrac{\text{MW}}{\text{Hz}}\right] = \sum_{i=1}^{N} D_{l,i} \tag{2.18}$$

$$\boldsymbol{D_{l,tot}}\ \left[\tfrac{\%}{\text{Hz}}\right] = \frac{D_{l,tot}}{\sum_{i=1}^{N} P_{load,i}} \cdot 100 \tag{2.19}$$

$$\boldsymbol{D_l}\ \left[\tfrac{\%}{\%}\right] = \frac{1}{2}\boldsymbol{D_l}\left[\tfrac{\%}{\text{Hz}}\right] \tag{2.20}$$

2.6 Secondary Control

After Primary Control has taken full effect and all interconnected areas are assisting the affected area in coping with the outage, the Secondary Control loop steps into action.

As mentioned previously, the two goals of Secondary Control are to restore the frequency and the tie-line power flows to their pre-disturbance values[8]. This makes Primary Control reserves available for another disturbance. It is necessary for the Secondary Control to act more slowly than the Primary Control, so that the control behavior is decoupled from the fast turbine dynamics and influences from the Primary Control. This is most often achieved by implementing the Secondary Control loop as a PI-controller with a large time-constant of up to several minutes.

In most interconnections, Secondary Control is invoked only by the area

[8]Secondary Control is often also used for Time Control purposes [3]. To achieve this, the frequency setpoint is adjusted to have a value slightly different from the nominal frequency to make up for accumulated deviations. In RGCE the coordination for the entire interconnection take place at swissgrid in Laufenburg.

causing the disturbance, by means of automatic generation control. This mechanism will be covered in more detail in chapter 3.

2.7 Tertiary Control

As seen in figure 2.2, Tertiary Control is most often manually activated by the operator of the area causing a disturbance. In the event of a large disturbance, Tertiary Control reserves can support the Secondary Control in restoring frequency and tie-line flows, particularly in cases where the Secondary Control reserves are exhausted. When Secondary and Tertiary Control have successfully reestablished the nominal frequency, Tertiary control also makes Secondary Control reserves available again by changing the scheduled operating points of area power plants participating in Tertiary Control.
The only requirement concerning Tertiary Control outlined in the UCTE OpHB states that these reserves must be sufficent to cover the largest expected loss of power in the area.
Tertiary Control is not discussed further because it is manually activated and because it does not affect the Automatic Generation Control (AGC) operations below.

Chapter 3

Automatic Generation Control

3.1 Classic Automatic Generation Control

By returning the frequency to its nominal value and the tie-line powers to their scheduled levels, AGC frees up Primary Control reserves and reestablishes the normal, pre-disturbance operation state. The classic implementation, which has been in use for several decades in many interconnections around the globe, consists of one AGC controller per control area, which centrally calculates a control signal $\Delta P_{AGC,i}$ for all generators participating in Secondary Control in its area[1]. The deviation from nominal frequency and scheduled tie-line power compose the Area Control Error (ACE) (see section 3.1.1). Thus, driving the ACE to zero is the goal of AGC. Figure 3.1 illustrates area 1 from figure 2.1 with AGC. The controller labeled AGC_1 measures the power flow on the tie-lines from area 1 to area 2 (P_{12}) and to area 3 (P_{13}), as well as the network frequency f. The nominal frequency f_{set} and the scheduled power flows of the tie-lines, $P_{12,sched}$ and $P_{13,sched}$, are used in the controller to calculate the deviation of the measured values. AGC is implemented as a PI-controller, according to equation (3.1). A small gain constant $C_{p,i}$ in the range of 0.1 to 1.0 and a large time constant $T_{N,i}$ in the range of 30 to 200 s as documented in [2] lead to a sufficiently slow increase in the control signal $P_{AGC,i}$. The large time constant stems from the fact that Secondary Control has to be sustained until it can be relieved by Tertiary Control, which often takes up to 15 min [4]. The speed of provision of Secondary Control power depends largely on the type and size of the generating units. While many hydro power plants can vary their power outputs over a large part of their output range within tens of seconds or

[1] This organisation scheme is referred to as "Centralised" by [3]. There are two schemes,"Pluralistic" and "Hierarchical", which work in a decentralised way. These are not discussed here but generally function along the same guidelines.

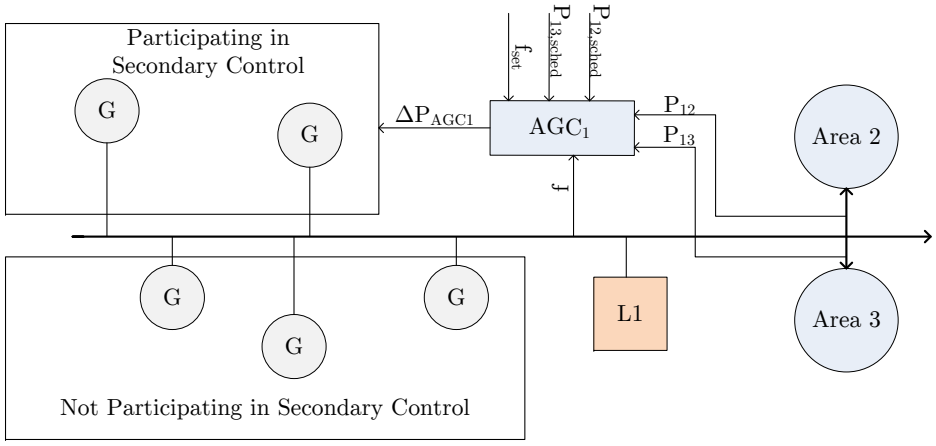

Figure 3.1: Area 1 Including the AGC Controller which sends the Control Signal ΔP_{AGC1} to all Generators Participating in Secondary Control.

minutes, coal-fired or nuclear plants employing steam turbines have longer activation times, in the range of a few minutes [8]. In addition to the activation time, different power plant types also feature distinctive dynamics in their power outputs. A large integration time constant in combination with a small proportional gain make the controller robust against tracking these short-term dynamics.

$$\Delta P_{AGC,i} = -(C_{p,i} \cdot ACE_i + \frac{1}{T_{N,i}} \int ACE_i \cdot dt) \tag{3.1}$$

3.1.1 Linear Area Control Error

The sum of all deviations between the actual tie-line power exchange from area i to j, P^j_{Ti}, and their scheduled values $P^j_{Ti,0}$ added to the weighted difference between the momentary frequency f and the setpoint frequency f_{set}[2] makes up the ACE as shown in equation (3.2). The weighting factor K_i is called "frequency bias factor", and determines the conversion from frequency deviation to power deviation and is given in [MW/Hz][3]. Ω_i is defined as the set of areas connected to area i.

$$ACE_i = \sum_{j \in \Omega_i} (P^j_{T,i} - P^j_{Ti,0}) + K_i \cdot (f_i - f_{set}) \tag{3.2}$$

It is known from measurements and calculations that the assumption of an identical frequency everywhere in a synchronized grid is not correct dur-

[2] f_{set} is equal to the nominal frequency f_N except at times when accumulated network time error is compensated by slightly increasing or decreasing the frequency.

[3] Different literature refers to the frequency bias factor in different ways. It is common to find a factor of $-B$, $-10B$ or $+B$ instead of the K_i which is used here.

ing dynamic phenomena. Based on [8] however, we can assume that the dynamics leading to different frequencies f_i in different areas (i.a. electromechanical transients and intermachine oscillations) act on much smaller time-scales than AGC itself and are filtered out by the AGC controllers, thus allowing the assumption of equation (3.3).
Using equation (3.3), together with the definition of total change in tie-line power flow out of an area i given in (3.4) and the definition of deviation of the measured frequency from the setpoint frequency in (3.5), the ACE for area i can be simplified to (3.6).

$$f_i = f \ \forall i \tag{3.3}$$
$$\Delta P_{Ti} = \sum_{j \in \Omega_i} (P^j_{Ti} - P^j_{Ti,0}) \tag{3.4}$$
$$\Delta f = f - f_{set} \tag{3.5}$$
$$ACE_i = \Delta P_{Ti} + K_i \Delta f \tag{3.6}$$

3.1.2 Non-Interactive Control

According to [2], any positive value of K_i in the ACE equation (3.6) in combination with an integrating AGC controller, such as given in equation (3.1) will guarantee that all ACE_i will eventually be controlled to zero.
The exact value of the frequency bias factor K_i is given by the "Non-Interactive Control" principle, which states that only the area responsible for a disturbance has to provide Secondary Control power to relieve Primary Control reserves and restore the nominal frequency.
Assuming now that a synchronous grid, consisting of N areas labeled $1 \dots N$, is subject to a change in load of ΔP_{load} in area l. From section 2.4 it is known that the Primary Control in all areas will act jointly and that the frequency will settle at a steady state differing by Δf_{ss} from the setpoint frequency according to equation (2.13). The individual contribution in stabilizing the frequency of every area is composed of its Primary Control power and of its loads' self-regulation effect and is transferred to area l via tie-lines[4]. The change in tie-line power $\Delta P_{T,i}$ all areas $i \neq l$ is calculated as shown in equation (3.7) and equation (3.8).

$$\Delta P_{T,i} = -(\frac{\Delta f_{ss}}{S_i} + \Delta f_{ss} \cdot D_{l,i}) \ \forall i \neq l \tag{3.7}$$
$$= -\Delta f_{ss} \cdot \beta_i \tag{3.8}$$

The sum of tie-line power flows and thus also the sum of tie-line power flow changes, as written in equation (3.9), have to equal zero in order to

[4]If some areas do not have a direct connection to l, the power will flow through intermediate areas. $\Delta P_{T,i}$ of the intermediate areas will not be affected by the this transit because inflow and outflow cancel out.

comply with the conservation of energy. From this, it is clear that the total change of tie-line power into the affected area l of $-\Delta P_{T,l}$ is obtained by summation of all other areas' contributions, as shown in equation (3.10). Inserting equation (3.8) into equation (3.10), $\Delta P_{T,l}$ can simply be written as equation (3.11).

$$\sum_{i=1}^{N} \Delta P_{T,i} = 0 \tag{3.9}$$

$$\Delta P_{T,l} = -\sum_{i \neq l} \Delta P_{T,i} \tag{3.10}$$

$$= \Delta f_{ss} \sum_{i \neq l} \beta_i \tag{3.11}$$

Using these deviations in tie-line powers, the ACEs of all areas, before Secondary Control is activated, can be calculated by inserting equation (3.8) and equation (3.10) into equation (3.6) resulting in equation (3.12) and equation (3.13).

$$ACE_i = \Delta f_{ss} \cdot (-\beta_i + K_i) \; \forall i \neq l \tag{3.12}$$

$$ACE_l = \Delta f_{ss} \cdot (\sum_{i \neq l} \beta_i + K_l) \tag{3.13}$$

To fulfill the Non-Interaction Control principle, the ACEs of all areas except for area l have to be zero, so that their AGCs do not react to the disturbance in area l. From equation (3.12) it is obvious that this can be implemented by selecting the frequency bias factor K_i according to equation (3.14).

$$K_i = \beta_i = \frac{1}{S_i} + D_{l,i} \tag{3.14}$$

The ACE of area l, using $K_l = \beta_l$, can be calculated by inserting equation (2.13) into (3.15), resulting in equation (3.16).

$$ACE_l = \Delta f_{ss} \cdot \sum_{i} \beta_i \tag{3.15}$$

$$ACE_l = -\Delta P_{load} \tag{3.16}$$

At first glance, this solution looks deceptively simple. To setup their frequency bias factor, every area has to add up its Primary Control generators' speed droops as shown in equation (2.15) and calculate its load damping factor according to equation (2.17).

As explained in section 3.1, AGC works on a slower timescale than Primary Control. It can be assumed that these two mechanisms are uncoupled, meaning that for every change $\Delta P_{AGC,l}$ in AGC power applied in area l, the

quasi steady state of Primary Control will be reached before the next change in $\Delta P_{AGC,l}$ is applied. Using this assumption, the frequency deviation after deployment of AGC power in area l follows from equation (3.17). It also implies that the ACEs of all areas $i \neq l$ will remain zero, while ACE_l will decrease according to equation (3.18).

$$\Delta f_{ss} = \frac{-\Delta P_{load} + \Delta P_{AGC}}{\beta} \tag{3.17}$$

$$ACE_l = -\Delta P_{load} + \Delta P_{AGC} \tag{3.18}$$

3.2 Current Practice in the RGCE

The legal framework for Primary and Secondary Control in ENTSO-E's RGCE is currently dictated by Policy 1 of the 2009 UCTE OpHB [3]. Further explanations of Policy 1 can be found in the appendix of the 2004 UCTE OpHB [4].

3.2.1 Network Characteristic Method

During normal operations[5], referred to as "Frequency Power Network Characteristic Method", Policy 1 requires every Transmission System Operator to implement a classic AGC according to chapter 3, which has to start operating no later than 30 s after a disturbance occurred and bring the ACE to zero without overshoot in no more than 15 min.
Estimation of RGCE's total frequency response characteristic β, referred to by UCTE and ENTSO-E records as λ_u, is currently done "on a regular basis" as specified in OpHBs 2004 [9] and 2009 [3]. Apart from these updates, usually occurring less than once per year, "it is taken to remain as constant as possible".

3.2.2 Change in Load-Frequency Control Policy

The 2004 UCTE OpHB defines the K-factor for every control block or area by a specific formula (3.19). The "contribution coefficient" c_i, defined as the ratio of electrical energy produced in area i over the total production in the interconnection in one year[6], is used to split the total frequency response characteristic among its areas. An additional factor of 10% is introduced to account for uncertainties in the self-regulation effect, assuming that overestimation of the frequency response characteristic is preferable. The overall network frequency characteristic λ_u of 18000 MW/Hz is composed of the

[5] Other modes of operation are only activated in case of equipment outages or emergency conditions.

[6] The factor c_i is also used to determine an areas share of the 3000 MW Primary Control reserves every year.

Primary Control speed droops, which are calculated according to the rule that the total Primary Control reserve of 3000 MW has to be provided within 200 mHz, and the load self-regulation effect of 1 %/Hz.

$$K_{ri} = 1.1 \cdot c_i \cdot \lambda_u \tag{3.19}$$

Since, by OpHB definitions, none of the factors in equation (3.19) change on an interval shorter than one year, the frequency bias factor of every area is supposed to stay constant for that same interval.
The revised OpHB policy on load-frequency control[7], approved in March 2009, states in its "Standards" section that "Frequency Gain Setting [...] shall reflect the best approximation of the real Network Power Frequency Characteristic of the Control Area/Block". It further postulates that the K-factor calculated by multiplying c_i and λ_u shall serve as the default value for the frequency gain setting according to equation (3.20).

$$\lambda_i^{default} = c_i \cdot \lambda_u \tag{3.20}$$

The calculation, however, must be adjusted in case of border-crossing trading in Primary Control reserves. The computation of the λ_u also changed significantly from the 2004 OpHB, resulting in an overall network frequency response of 26680 MW/Hz for 2009. In addition to the Primary Control reserves from equation (3.21) and the self-regulation effect from equation (3.22), which made up λ_u in the previous OpHB, two new components ${S_{additional}}^{-1}$, equation (3.23), and ${S_{surplus}}^{-1}$, equation (3.24), are added in the 2009 version. The first accounts for the fact that Primary Control delivers on average 30% more power per frequency than it is planned to. The latter is referred to as "surplus-control of generation", and is briefly explained to originate from a linear frequency dependency, according to figure 3.2, of roughly 50% of the generators in the network. To the knowledge of the author, no published measurements or analyses as to the exact size or cause of both of these effects currently exist. The most probable explanation of the "Additional Primary Control" is incomplete adjustment of speed droop controllers, which are especially hard to modify in older generators. According to swissgrid, many power plant owners chose not to readjust their turbine controllers to lower settings even when not taking part in the official Primary Control reserves. Other operators, instead of completely switching off the speed droop controllers, set the controllers' deadbands to large values of over ± 200 mHz. While both of these measures complicate the calculation of the actual Primary Control behavior, they are beneficial to the performance of the whole interconnection in the event of disturbances.
The result of the sum of these four effects is the overall network frequency

[7] Load Frequency Control (LFC) is a synonym for AGC, which is used throughout the UCTE OpHB.

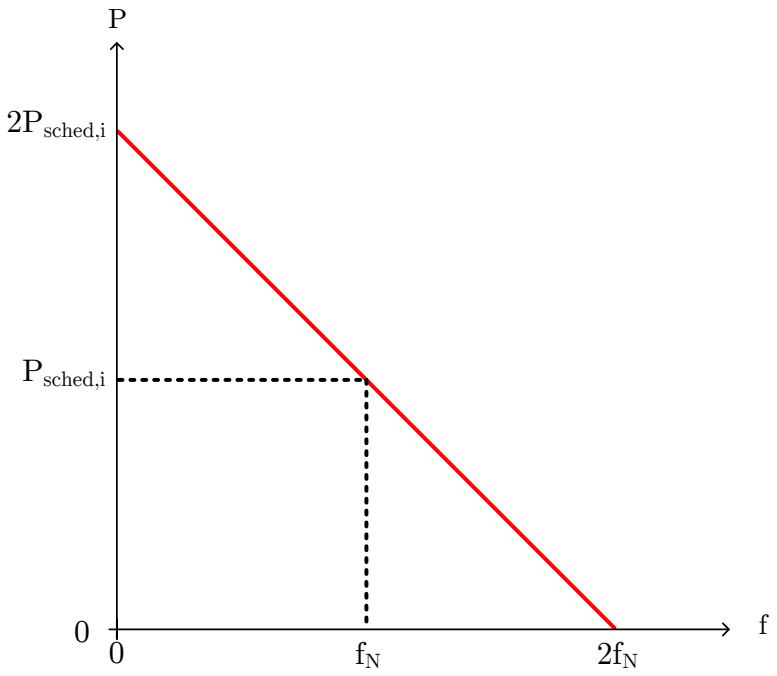

Figure 3.2: $\frac{100\%}{50\,\mathrm{Hz}}$ Linear Frequency Dependency which 50% of the Generators are Following According to the OpHB.

response as shown in equation (3.25).

$$\frac{1}{S_{prim}} = \frac{3000\,\mathrm{MW}}{200\,\mathrm{mHz}} \tag{3.21}$$

$$D_l = 1\,\frac{\%}{\mathrm{Hz}} \cdot P_{load}^{highest} \tag{3.22}$$

$$\frac{1}{S_{additional}} = 0.30 \cdot \frac{1}{S_{prim}} \tag{3.23}$$

$$\frac{1}{S_{surplus}} = \frac{50\%}{50\,\mathrm{Hz}} \cdot P_{generation}^{mean} \tag{3.24}$$

$$\lambda_u = \frac{1}{S_{prim}} + D_l + \frac{1}{S_{additional}} + \frac{1}{S_{surplus}} \tag{3.25}$$

Compared to the stringent definition of the frequency bias factor by formula in the earlier version of the OpHB, the new standard leaves some room for interpretation. From the definition of the ACE according to equation (3.6) it is clear that the frequency bias factor K_i has to be changed if Primary Control reserves are traded over borders of areas, which is explicitly specified in the OpHB. It is not entirely clear from the new standard whether or not cross-border trading is the only case where changing K_i is allowed. A plausible interpretation is that any method yielding a better approximation

of the actual frequency response characteristic β_i than equation (3.25), is allowed.

3.2.3 Measurements of Performance

As previously stated, the main target of Secondary Control as defined in the 2009 UCTE OpHB is returning the system frequency and the tie-line powers back to their set-points by reducing the ACE to zero with no overshoot, in under 15 min. There are a number of indicators used to measure the quality of Frequency Control employed in RGCE, as explained in [4]. During normal operation the monthly standard deviation σ of the frequency can be calculated by taking averages of the frequency over 15 min (f_l) and summing the squares as in equation (3.26).

$$\sigma = \sqrt{\frac{1}{n} \cdot \sum_{i=1}^{n} (f_l - f_0)^2} \tag{3.26}$$

Also the number and duration of frequency deviations of more than 50 mHz from the frequency set-point must be measured.
In case of generation or load loss of more than 1000 MW, categorized as large disturbance, the recovery of the system frequency by Secondary Control is compared to a trumpet-shaped curve of the form $H(t) = f_0 \pm A \cdot e^{-t/T}$. The parameters A and T are calculated from a number of constants, the 15 min maximal recovery time and the size of the disturbance P_a; f_0 is the pre-disturbance frequency. When the system frequency stays within the boundaries given by $H(t)$ during recovery back to f_0, the Secondary Control mechanism is deemed satisfactory. Figure 3.3 from [4] shows trumpet-curves for different disturbance sizes.

3.3 Proposed Improvements and New Schemes

Since the introduction of AGC more than half a century ago, its shortcomings have been well documented (see section 4.1) and a large number of alternatives have been proposed by different parties. In 2005, Ibraheem et al. categorized and summarized 184 different sources in "Recent Philosophies of Automatic Generation Control Strategies in Power Systems" [10]. This extensive literature review provides a well informed overview of the different approaches taken to simulate the effects of AGC, to improve on the current implementations and to completely redesign Secondary Control.

3.3.1 Changes to Classic AGC

In [11] Quazza 1966, it is suggested that selecting $K_i = \beta_i$ in all areas of an n area system fulfills the non-interaction principle between frequency and tie-

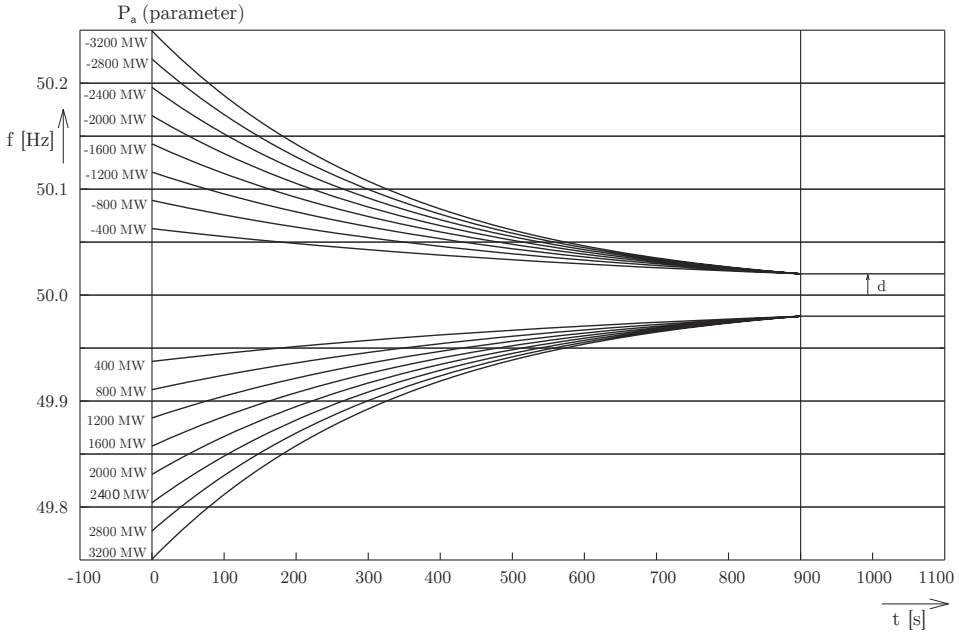

Figure 3.3: Trumpet-Curves for Different Incident Sizes P_a.

line power, as well as the principle of non-interaction between different areas (at least for the low-frequency approximation). However, there was and still is research and development carried out to improve the simple control given by equation (3.1) and equation (3.6).

Some early research about the fundamentals of AGC, such as that carried out by Elgerd and Fosha [12], applied new concepts of control theory, in the case of [12], the theory of optimal control, and suggested that β might not be the best choice of frequency bias factor K_i. These suggestions, however, were never utilized.

At the same time, other research looked into expanding the basic definition of ACE given in equation (3.6) by adding power system properties other than tie-line flow and frequency deviation. One example of this is [13], in which Cohn makes a case for adding two terms accounting for the accumulated inadvertent energy exchange between areas and for the deviation of the grid time from real time.

Since there are a number of sources of estimation errors when determining a system's frequency bias response (see section 4.1), a necessary method to improve classic AGC is by modeling K_i as closely as possible to the actual frequency response characteristic β. To achieve this, Kennedy et al. in 1988 in [14], proposed a non-linear frequency bias factor K_i. The goal of the non-linearity was to emulate turbine governor dead-bands which were known to

violate the assumption of linear speed droop control[8]. Another approach consisting of an adaptive filter for online updating of β was proposed by Chang-Chien in the publications [15] and [16].

3.3.2 Fundamentally New AGC Schemes

With the advent of control theory, a large number of AGC implementations, partially or entirely different from the algorithm described in section 3.1, were developed and simulated. Control methods such as neural networks, fuzzy logic and genetic algorithms have been applied to the problem of AGC with varying degrees of success. Again, [10] provides an overview of the extensive, ongoing research in these areas prior to the year 2005.
The article "Understanding Automatic Generation Control" by N. Jaleeli et al. [8], and the substantial discussion following its publication in 1992, portrayed fundamental redesigns of AGC in a critical light. The main objections to these redesigns were that they violate fundamentals of electric power systems or the goal of AGC itself. It was observed that many approaches to AGC redesign neglected power plant dynamics and their shortcomings (i.a. non-linearities, limited control range and speed), while others neglected the long decision cycle times typical for AGC. Another flaw found by Jaleeli et al. in many publications, was the level of detail used in the simulation of new AGC schemes. Many of them involved dynamic phenomena, such as tie-line interchanges due to frequency deviations between control areas, that occur on a much smaller time-scale than AGC actions. Yet another point of criticism was the assumption of many publications that new AGC schemes could be introduced in an entire interconnection at once. It was pointed out by Jaleeli et al., that especially the large interconnections of North America and Europe have grown evolutionarily and classic AGC has been at least partially implemented for over six decades. Changes to these systems can thus only be established slowly and continuously.

3.3.3 Example of New Implementations outside ENTSO-E

With the ongoing expansion of interconnections and the growth of electric power grids in certain parts of the world, AGC is currently becoming predominant in areas which previously did not employ Secondary Control or manually dispatched reserves via an operator.
An example of newly adopted classic AGC can be found in [17]. The area in question is the country of Montenegro which previously contracted out Secondary Control to Serbia and has now established its own AGC. In the report, Stojkovic presents insights into the details of Montenegro's AGC in-

[8]Even the newest UCTE OpHB regulations require turbine governors to have the smallest possible deadband, illustrating the persistence of this issue with linear frequency bias factors.

cluding noise management and individual generator dispatch.
When Africa's largest power producer, ESKOM, redesigned its frequency control in order to reduce generator activation, classic AGC was already implemented in the system but performed unsatisfactorily. A complete analysis of the frequency control policy in action at the time lead to numerous changes, such as widening of the Primary Control deadbands [18]. Additionally the ACE calculation of the existing AGC was changed from the established equation (3.6) to a fuzzy-logic algorithm which includes the standard ACE as well as its derivative ΔACE, as presented in [19]. ESKOM claims in [18], that its frequency policy and control redesign reduced daily generator activation by as much as 80 % without any implications to their customers. These results have to be weighed against the unique situation ESKOM finds itself in, being by far the largest energy producer in a sparsely interconnected grid.
The change of measurements of control performance by the North American Electric Reliability Council (NERC) in 1997 triggered rethinking of the employed AGC algorithms in most of the North American interconnections. 'AGC Logic Based on NERC's New Control Performance Standard and Disturbance Control Standard' [20] by Yao et al. proposed a completely new AGC controller which specifically optimizes its output for a maximum compliance with NERC's new performance indicators. ACE according to equation (3.6) is still used in this controller but only to constantly calculate the area's current performance indicators rather than defining the control goal. The comparison of these real-time measurements with long-term values results in control actions to minimize the deviation from NERC's specifications. The promising results led Texas Utilities Electric Company and the University of Texas at Arlington to start developing a practical implementation according to [20]. However Jaleeli and VanSlyck were quick to point out that an optimization of performance indicators rather than the actual frequency and tie-line error can have unforeseen consequences for all connected areas, and that more simulation as well as research is needed before the application of the proposed control system [21].

3.3.4 Applicability to the RGCE and Switzerland

Though interesting, the approaches presented in the above sections 3.3.3 and 3.3.2 are unlikely to be adopted in the control areas of the RGCE in the near future. Member areas which have been interconnected strongly for several decades have invested considerable resources in the existing control system over the years. The classic scheme has proven to be reliable and dependable. Nevertheless some of the recently developed AGC systems will find their way into modern electric power systems which have serious problems with their current implementation or have no AGC at all.
It has therefore been decided, for the scope of this project that the ap-

proach with the greatest relevance is to build on the existing Secondary Control scheme of AGC with the ACE calculation explained above and to improve on it solely by proposing a new strategy for the sizing of the frequency bias factor K. This change to the algorithm is small enough that it can be incorporated easily into the existing system. This approach also allows direct comparison between the proposed and the classic system since it does not require large changes to the existing control architecture. Additionally, the availability of research on the topics of non-linear frequency bias settings and interconnection frequency response characteristics assures a well-founded starting point.

Chapter 4

Estimation Errors of β

As explained in section 3.1, the basis of the AGC scheme currently implemented in RGCE is the Non-Interactive control principle, which specifies that only the area in which a disturbance occurred should provide Secondary Control power to restore pre-disturbance conditions. It is, however, evident from the presented equations that if an area cannot set its frequency bias factor K_i to be exactly equivalent to its frequency response characteristic β_i, the Non-Interaction principle will be violated.

4.1 Sources of Estimation Errors

4.1.1 Assumptions of Classic AGC by the RGCE

The calculation of the frequency bias factor of any area according to the the definition given by the OpHB 2004 and 2009, albeit different in their composition, are based on the following four fundamental assumptions.

1. The frequency response characteristic β (called λ_u in the OpHB) of the entire interconnection is
   (a) calculable from two to four known constituents and
   (b) remains constant for at least one year.
2. Every area's individual frequency response characteristic β_i can be calculated by multiplication of the characteristic of the whole network with a contribution factor c_i.
3. This contribution factor c_i is equal to an area's share of the annual energy production of the interconnection and remains constant over the course of one year.
4. β and its constituents are linear (i.e. independent of the frequency).

4.1.2 Research Performed in the Union for the Coordination of Production and Transmission of Electricity (UCPTE)

Soon after implementing AGC with ACE, the operators of UCPTE encountered a number of difficulties. The UCPTE annual reports 1957-1958 [22] and 1958-1959 [23] cover in great detail the problem of determining the frequency response characteristic in the network which then connected Belgium, West Germany, France, Italy, Luxembourg, the Netherlands, Austria and Switzerland. At first β was estimated by summation of the linearized speed droops of all participating power plants, as explained in section 2.5[1], however measurements of the frequency response characteristic of the network showed that it never reached more than a fraction of the calculated value. One explanation was found to be power plant protection equipment such as oil-breaks and opening-limiters which added non-linearities and time-dependencies to the speed droops. They also hindered certain power plants (i.a. hydro power plants with opening limiters) from contributing to Primary Control if they could do so at all. Subsequently, two improvements were proposed to increase the frequency response characteristic, thus making the frequency less susceptible to load changes. These were to deactivate some of the protection equipment and to equip power plants with more accurate controllers in order to reduce deadbands as well as measuring insensitivities.

The first measurements listed in [22] to determine the whole interconnection's β were done in May 1957 by switching off two generators in the afternoon and two pumps at night, each generator and pump making up about 1 % of the UCPTE generation and load at the time. The results showed β values of 13.1 % and 13.5 % during the day as well as values of 11.8 % and 11.9 % during the night. Over the two years following these initial tests, many more were executed in most UCPTE member areas to determine the individual areas' frequency response characteristics.

The results published in 1959 in [23] demonstrated measured β_i over a wide range for the different areas, which was explained as stemming from the different types and sizes of power plants prevalent in the different areas. It was also found that the characteristics changed depending on the time of day the measurement was taken. This was also explained to be attributable to power plant scheduling depending on the amount of the load. The fact that different types of power plants exhibit different speed droops has been covered widely in literature; as one example, the ranges of S for the three most prevalent types of power plants are listed in [24] as being 4 to 6 % for nuclear power plants, 4 to 6 % for conventional thermal power plants and 2 to 6 % for hydro power plants.

With the increasing size of the UCPTE interconnection, measuring network

[1] Whether or not the self-regulation effect of the loads was included as well is not exactly specified in the report; the focus clearly lay on the generators.

parameters by switching off large generators or loads in order to find β was deemed unsecure as well as unnecessary because naturally occurring faults provided readily available data for analysis. A comprehensive evaluation published in the annual report of UCPTE in 1982 [25] analyzed 1251 faults over the course of five and a half years. A high dependence of the frequency response characteristic on the season, the weekday and the hour of the day was found. Figure 4.1 from [25] shows the development of the monthly average of the frequency response characteristic β in the upper curve and the monthly maximum load in the lower curve. It is obvious from this figure

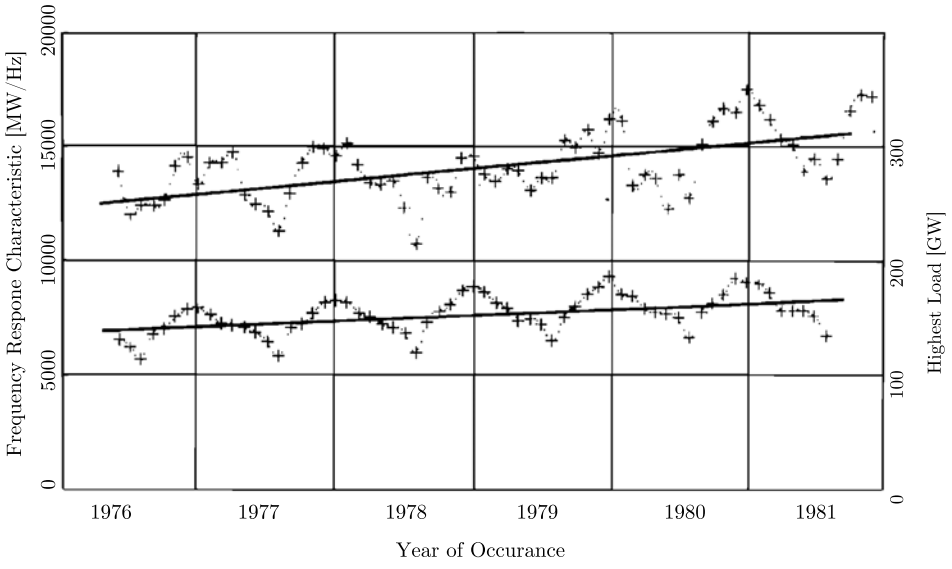

Figure 4.1: Monthly Average of Frequency Response Characteristics and Maximum Load in UCPTE. Upper Curve: β Using the left Scale of [MW/Hz]. Lower Curve: Monthly Maximum Load, Using the right Scale of [GW]. Actual Measurements are Given by '+'; Dotted Lines are Spline-Interpolation; Solid Line Indicates Linear Regression.

that assumption 1b is violated because β shows a significant seasonality. That said, there is a noticeable correlation between the frequency response characteristics and the total load of the network. The report explains the seasonalities as an effect of the different types of power plants running at different times of the day, week, and year depending on the demand by the loads. The same measurements presented in figure 4.1 were also analyzed for the time of day the fault occurred. Figure 4.2 shows all of the 1251 measured characteristics. Despite the noise stemming from the different times of year when the incidents took place, a tendency of the frequency response characteristic to be higher during peak-load (between hours 6 and 18) can be discerned. Also in this case, the explanation was found in the additional peak power plants which were online during the high-load hours.

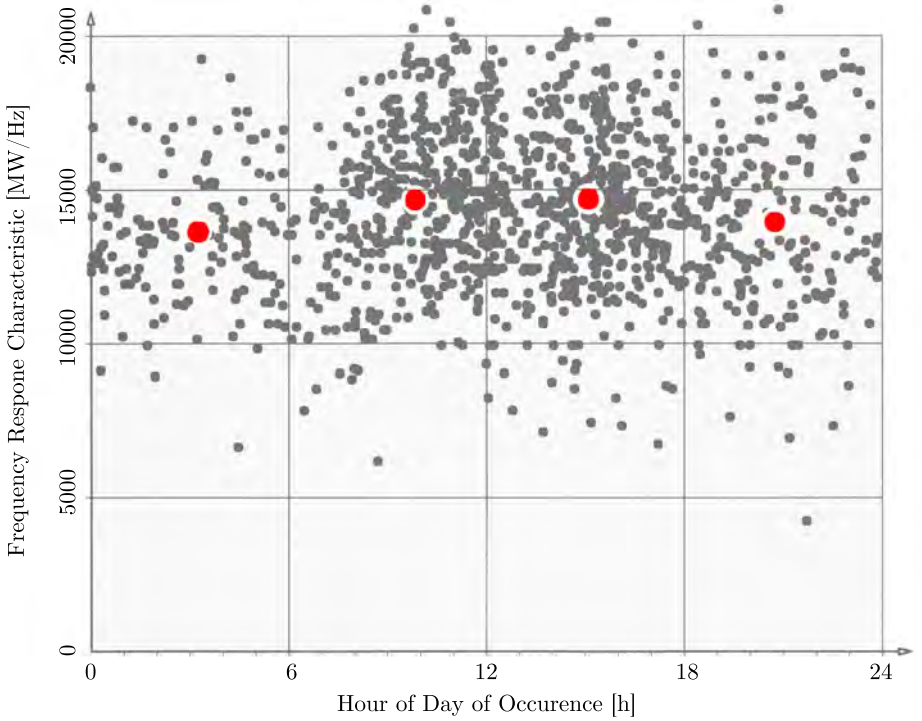

Figure 4.2: Time of Day of the Measured Frequency Response Characteristics. Averages Over Five Years in Red.

In [26], H. Weber et al. evaluated the continued measurements of disturbances larger than 600 MW in the UCPTE grid between 1988 and 1996. The absolute values of β showed the same trends as previously described, i.e. a considerable seasonality and a net increase with overall system growth. When calculating the frequency response characteristic relative to the total load of the system ($\boldsymbol{\beta}$) however, the effects of seasons and the growth of the network became much less dominant, as displayed in figure 4.4. Between 1988 and 1991 the average $\boldsymbol{\beta}$ exhibited little change between summer and winter. This change increased considerably after 1991, when according to Weber et al., some operators stopped to adjust their Primary Control reserves according to their total energy production. Albeit not mentioned in the report, it can be assumed from earlier findings that the change in types of power plants being online during winter or summer also has some influence. In addition to the development of the mean values, it has to be noted that the actual measurements tend to differ greatly from the average, leading to large standard deviations.
In many of the previous reports it was assumed that the frequency response of the system was linear, so that it can be calculated from any measurement simply by calculating $\Delta P_{load}/\Delta f_{ss}$. Figure 4.3 shows 1285 disturbances, which occured between 1988 and 1995 in the UCPTE network and 31 disturbances in 1995-1996 after UCPTE and Former synchronous area covering Czech Republic, Hungary, Poland and Slovakia (CENTREL) were connected. It can be seen from the figure that a linear approximation is possible but many datapoints with significant deviations exist. Figure 4.4 shows the same analysis for the relative characteristic, which features a better correlation between the linear approximation and the 1316 measurements. This analysis adds some credibility to assumption 1b, under the conditions that relative $\boldsymbol{\beta}$ is referred to and that the linearity is only an approximation.
From the detailed analysis of the frequency bias factor in the UCPTE, over a period of four decades, it can be concluded that two of today's basic assumptions are erroneous: β of the Central European interconnection is neither constant over any period of time, nor is it exactly linear. It was shown, however, that β can be measured retroactively by measuring the effect of normally occurring disturbances on the frequency.

4.1.3 Non-Linearities from Generators

Even though turbine governors might use a linear speed droop such as that shown in figure 2.3, the various non-linear elements in the control path between the governor and the actual power output result in a non-linear overall speed droop characteristic $S(f)$ for any generator. Figure 4.5 from [1] shows a simplified comparison of the ideal, linear speed droop compared to the non-linear speed droops of steam and hydro power plants.

A second source of non-linearities in the speed droop of a generator is its

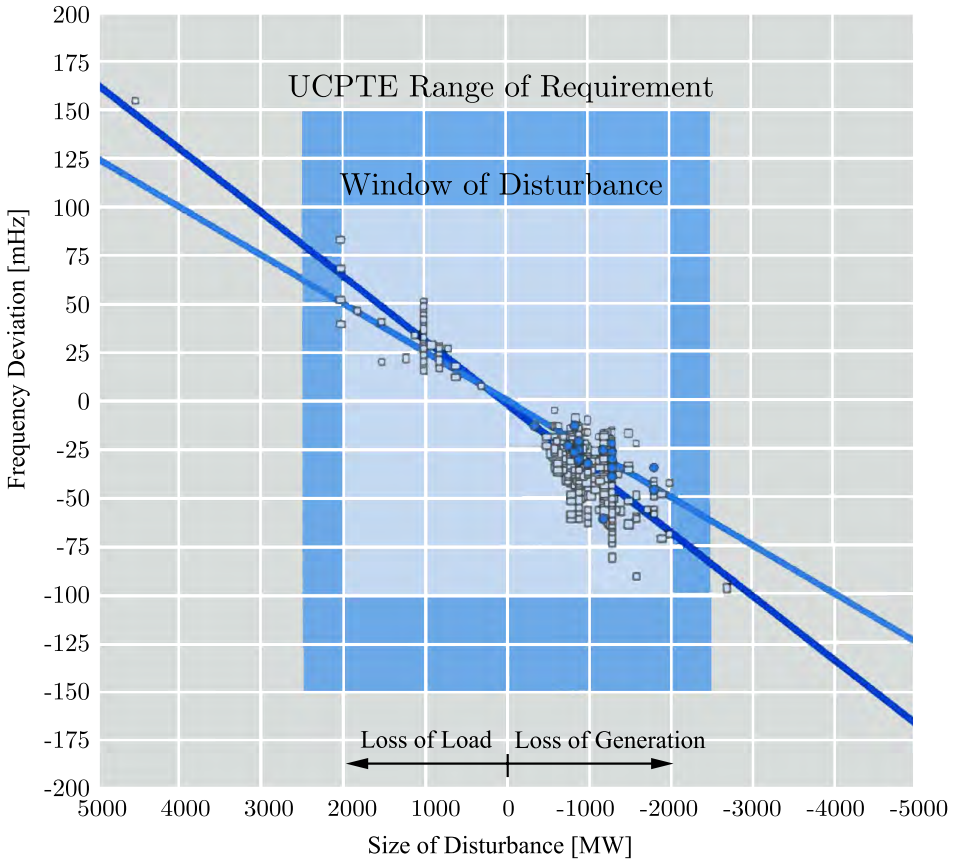

Figure 4.3: Frequency Deviation in mHz per Loss of Load in MW. White Squares: 1285 Disturbances between 1.1.1988 and 17.10.1995 in UCPTE; Blue Circles: 31 Disturbances between 19.10.1995 and 10.2.1996 in UCPTE with CENTREL; Dark Blue Line: Linear Regression of White Squares $\beta_{UCPTE} = 30000\,\mathrm{MW/Hz}$; Light Blue Line: Linear Regression of Blue Circles $\beta_{UCPTE+CENTREL} = 40000\,\mathrm{MW/Hz}$. [26]

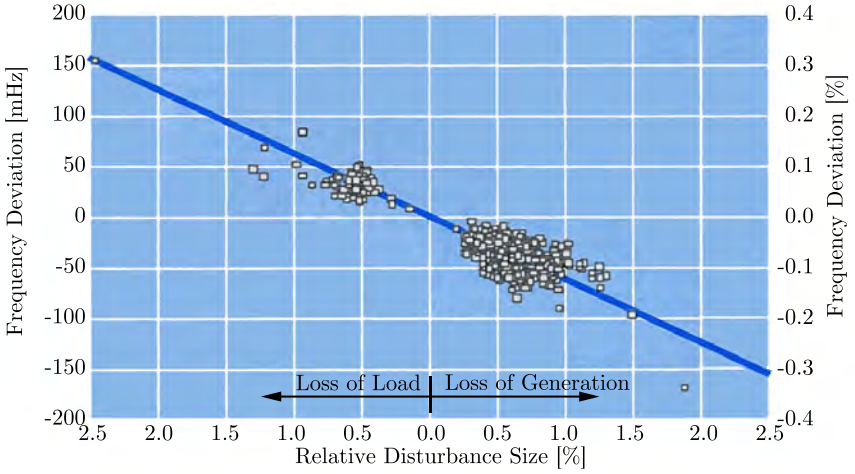

Figure 4.4: Frequency Deviation in mHz (Left Scale) and % of 50 Hz (Right Scale) per Loss of Load in % of Total Load. White Squares: 1316 Disturbances between 1.1.1988 and 10.2.1996; Dark Blue Line: Linear Regression of Measurements with $\beta = 13\,\%$. [26]

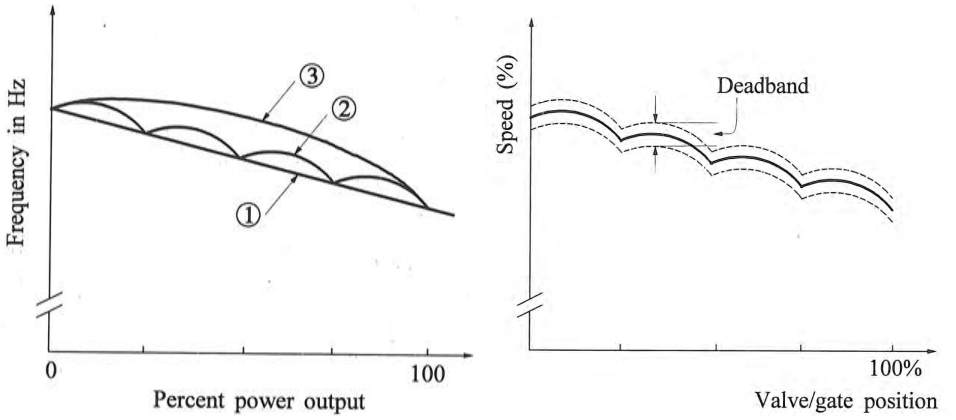

Figure 4.5: Left: Comparison of the Ideal, Linear Speed Droop Characteristic (1) to the Typical Speed Droops of a Thermal Power Plant (2) and a Hydro Power Plant (3). Right: Typical Speed Droop of a Thermal Power Plant with Added Deadband.

deadband. The deadband of a generator, illustrated in figure 4.5, is defined as "the percentage of steady-state speed within which no change in the position of governor-control valves or gates occurs" [1]. The position of the generation within its deadband previous to a disturbance has been found to be randomly distributed [27], which was found to lead to a significant overall decrease of a network's frequency response characteristic [28]. Continuing improvements of governor technology (i.a. electrohydraulics) have led to significantly lower deadbands in new generation units. That the effect of deadbands still persists can be seen in the fact that the most recent version of the UCTE OpHB [3] specifies a maximal deadband of $\pm 10\,\mathrm{mHz}$ for any primary controller and requires control areas to offset their deadbands.

4.1.4 Contribution Factor c_i from UCTE Data

Since a network's total frequency response characteristic β can be determined statistically from naturally occurring disturbances, as shown above, it is used as a basis to calculate the individual frequency response characteristic of every control area in RGCE (assumption 2 from section 4.1.1). Said calculation is currently done on an annual basis according to every area's share of the total energy production over one year (assumption 3). It is clear that this approach only leads to valid results if an area's share of the total energy generation does not change over the course of the year.
To ascertain whether this assumption is reasonable, data from the RGCE section of the ENTSO-E Statistical Yearbook 2009 [5] has been compiled into figures 4.6 and 4.7. The first shows the contribution factors calculated

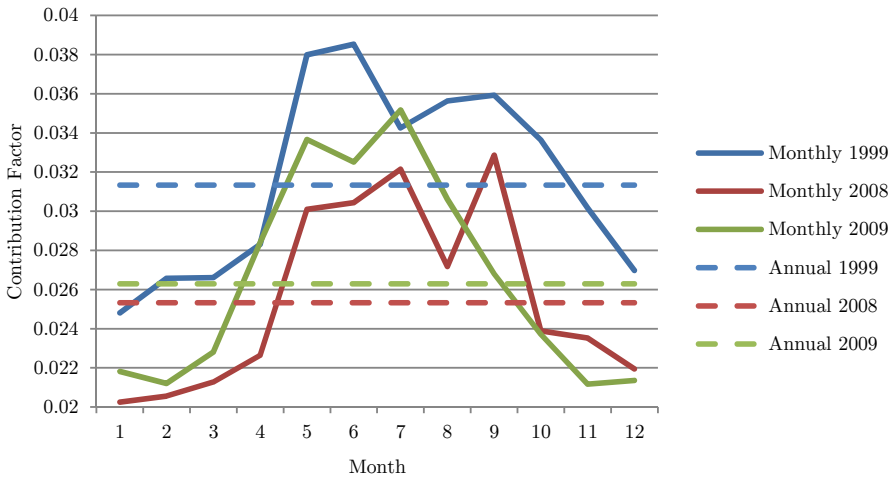

Figure 4.6: Contribution Factors c_i of Switzerland in RGCE, Calculated using Annual Averages (dotted) and Monthly Averages (Solid) in 1999, 2008 and 2009.

as specified by the UCTE OpHB, by dividing the annual electrical energy

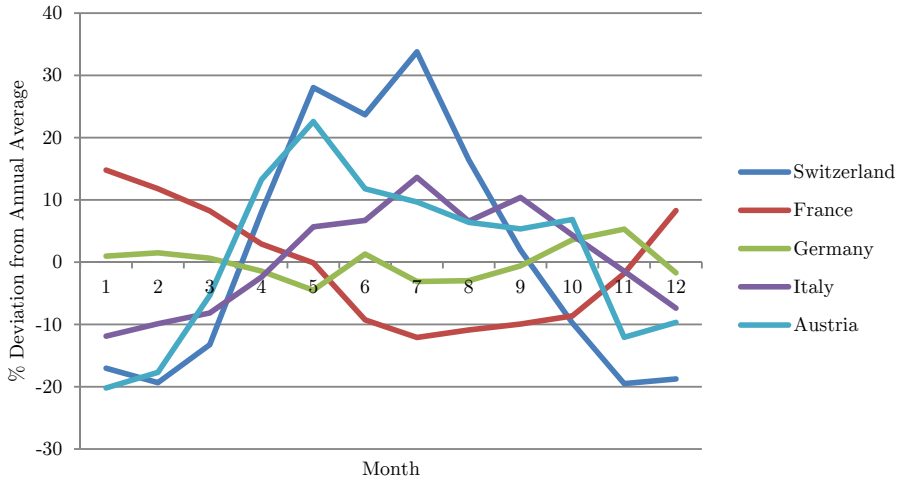

Figure 4.7: Deviations between Contribution Factors c_i Calculated on Monthly and Annual Basis for Switzerland an its Neighboring Countries in 2009.

production of the control area Switzerland by the total generation of RGCE (dotted lines). For comparison, the contribution factors were also calculated from the share of energy produced in Switzerland during every month of the same years (solid lines). It is evident from the figure that Switzerland's share of the total generation is much lower in the winter months than during the summer months. The monthly contribution factors deviate maximally 23 % in 1999, 30 % in 2008 and 34 % in 2009. The most probable explanation of this phenomenon is the fact that roughly two thirds of Swiss power production comes from hydro power plants which reach their peak power production in the summer months. Compared to other countries in RGCE this is a high fraction of season-dependent generation. As a result of this seasonality, the assumption of being able to determine an area's frequency response characteristic using a contribution factor which is constant over the time-scale of one year is invalid.
Figure 4.7 shows the percentage of deviation of contribution factors calculated on monthly bases from the ones calculated annually over the course of the year 2009. While Switzerland seems to incur the largest deviations over the course of 2009, Austria, Italy and France have months where their share on RGCE's total production differed by more than 10 % of the annual average. With the exception of Germany, figure 4.7 lends even more evidence to the non-applicability of assumption 3.

4.1.5 Research on Load Self-Regulation

Most of the fundamental literature on frequency control carries only very little information about the self-regulation effect of loads. Kundur [1] sim-

ply states that a fraction of the load is sensitive to changes in frequency and that the factor D_l is typically between 1 and 2 %/%, while Andersson [2] lists values between 0 and 2 %/% as plausible. The UCTE OpHB [3] assumes a constant self-regulation of 1 %/Hz or 0.5 %/% in the RGCE interconnection. The research about UCPTE's frequency response characteristic carried out in [26] determined the average β in the time between 1988 and 1996 to be around 8 %/%. In addition to the considerable standard deviation from this value, not being able to specify the load damping factor more accurately than being somewhere between 0 and 2 %/% adds even more uncertainty.
Two extensive reports by Welfonder et al., [29] and [30], show the results of a study of eight different measuring points in Germany over the course of up to two and a half years. The results indicated a similar seasonality of self-regulation as that already found in the frequency response characteristic. The main reason given is the fraction of motor loads in the total load. Motor loads generally consume less power at decreased frequency, while other loads such as ohmic heating are frequency insensitive. The effect of this can be seen in the fact that the average load-damping factor in summer was found to be roughly one third higher than the average in winter. Even larger differences were found between measurements during business hours and weekend, evening or night hours. In addition to the standard load-damping, which measures the change in active power consumption as a result of frequency changes, Welfonder et al. also included active power deviations resulting from voltage variations, which were a result of frequency changes. The annual average of the total load-damping resulting from frequency deviations in all seven areas was found to be 1.5 %/%, with the average in summer being 1.8 %/% and 1.2 %/% in winter.

4.2 Effects of Estimation Errors on Network Operations

Using equation (3.12) and (3.13), the initial responses of AGC controllers can be calculated for different frequency bias factors K_i. Table 4.1 shows the effects of different K_i on AGC of an area i for the case when area k causes a disturbance by loss of generation (second row) or loss of load (third row). It is clear that when K_i is set to be exactly equal to the frequency response characteristic β_i, no power change results from AGC action[2]. If this is not possible, it is preferable to chose K_i to be larger than β_i according to the second column, because area i supports the area in need. Situations where K_i is smaller than β_i should be avoided since the AGC of area i would worsen the disturbance by decreasing its power output in the case of missing generation and by increasing its power in the case of excess generation in

[2]The problems with fulfilling this non-interaction criterion were, however, presented above.

area k.

For an area causing a disturbance (area k in the example above), equation

Δf	$K_i > \beta_i$	$K_i = \beta_i$	$K_i < \beta_i$
$\Delta f < 0$	$ACE_i < 0$ $\Delta P_{AGC,i} > 0$ area i supports	$ACE_i = 0$ $\Delta P_{AGC,i} = 0$ no interaction	$ACE_i > 0$ $\Delta P_{AGC,i} < 0$ area i interferes
$\Delta f > 0$	$ACE_i > 0$ $\Delta P_{AGC,i} < 0$ area i supports	$ACE_i = 0$ $\Delta P_{AGC,i} = 0$ no interaction	$ACE_i < 0$ $\Delta P_{AGC,i} > 0$ area i interferes

Table 4.1: Effects of Different Frequency Bias Factors on AGC of an Area not Causing a Disturbance.

(3.13) shows that as long as K_k is chosen to be larger than zero, it will always lead to correcting AGC power changes.

To find a measurement for the power which is transferred from all areas i to an area k hit by a disturbance, N. Cohn defined the term "inadvertent interchange" in [31] as being composed of "primary inadvertent interchange" and "secondary inadvertent interchange". Primary inadvertent interchange I_{ii} of an area i stems from that area's non-ideal AGC, while secondary inadvertent I_{in} represents the control power which area i has to provide because of AGC-actions in area n. The definitions of "primary inadvertent" and "secondary inadvertent" both include Primary as well as Secondary Control power, as defined in chapter 2.

In the scope of this report, it is of interest to know how much power is transported over tie-lines to other areas as a result of an imperfect AGC, to obtain a measurement for unnecessary stress on these tie-lines. This can be calculated by integration of the absolute value of the tie-line power flow, which is the sum of Primary Control power, Secondary Control power and the load self-regulation effect, according to equation (4.1). This equation is a simplification of Cohn's primary inadvertent, neglecting measuring errors. Additionally, it is important to know the total energy produced by AGC alone over the time of a disturbance and if the AGC power supported the area in need or if it interfered. To make this difference, the AGC-signal $\Delta P_{AGC,i}$ can be split up in supporting power $\Delta P^{+}_{AGC,i}$ (i.e. when Δf and $\Delta P_{AGC,i}$ share the same sign, as seen in table 4.1) or interfering power, $\Delta P^{-}_{AGC,i}$, as shown in equation (4.2). To then calculate the corresponding energy, a simple integration from the start of the disturbance ($t = 0$) to the time the disturbance resolved ($t = T$) of the AGC-signal can be done as

demonstrated in equation (4.3).

$$W_{tie,i} = \int_0^T |\Delta P_{T,i}| dt \tag{4.1}$$

$$\Delta P^{\pm}_{AGC,i} = \begin{cases} \Delta P_{AGC,i}, & \Delta f \cdot \Delta P_{AGC,i} \leqslant 0 \\ 0, & otherwise \end{cases} \tag{4.2}$$

$$W^{\pm}_{agc,i} = \int_0^T \Delta P^{\pm}_{AGC,i} dt \tag{4.3}$$

Chapter 5

Deterministic, Semi-Online Sizing of K_i

Chapters 3 and 4 have identified a number of shortcomings of the currently implemented Secondary Control. A complete redesign of frequency control, such as proposed by some of the research presented in section 3.3, could potentially address most of the drawbacks of the established system but entirely retrofitting a vast and complex system which has grown evolutionarily over more than six decades requires substantial investments and long-term planning. Therefore, solutions that can be implemented in the short-term have to build on the existing control infrastructure and make use of the research performed in the past.

The presented approaches focus on deterministically estimating the current network frequency response β_i of an area i in order to set the frequency bias factor K_i of the AGC as close to β_i as possible[1]. In order to achieve this, the four following methods may be utilized.

5.1 Updating c_i Regularly

The simplest method of resizing K_i is the recalculation of an area's contribution factor c_i on an interval smaller than one year. The analysis performed in section 4.1.4 found differences of up to 30 % between annually and monthly calculated contribution factors. It is reasonable to assume that similar discrepancies can be found on shorter time frames as well[2]. Especially for an area such as Switzerland which has large pumped-storage power plants that act as generation during times of high load and as loads during times of low

[1] Some of the algorithms described in the following sections will contain specific details about a possible realization in Switzerland but should be easily adaptable to other control areas as well.

[2] Detailed data of production of electricity by area in ENTSO-E is only available as monthly averages.

electricity prices, c_i can change considerably over short intervals. In order to avoid interfering with the function of the AGC's integration component, an update interval considerably larger than the integration time-constant has to be selected. In addition to this restriction, the large frequency excursions regularly appearing around the hour mark further impose difficulties on the timing of updates.
It is thus proposed that update intervals coincide with European Energy Exchange (EEX)'s definition of peak and offpeak times. This results in three contribution factors each day. One for the twelve hours of high generation and load between 8:00 and 20:00 and two for the times of low generation and increased pump-load between 0:00 and 8:00 and between 20:00 and 24:00. To avoid interferences with AGC operations around the full hour, the actual update of the K-factor should occur 30 minutes before the beginning of each period.

Necessary for the calculation of the updated contribution factors $c_i^{l,m}$, where l and m stand for the first and last full hour covered by the factor, are the scheduled power generation levels $P_{G,j}^k$ for all areas j in the synchronous grid over the hours k of the following day. $c_i^{l,m}$ is calculated according to equation (5.1) by dividing the generation of area i by the total generation of all areas over the hours l to m. The frequency bias factor $K_i^{l,m}$ results from the multiplication of $c_i^{l,m}$ with the frequency response characteristic λ_u determined by ENTSO-E, as shown in equation (5.2).

$$c_i^{l,m} = \frac{\sum_{k=l}^{m} P_{G,i}^k}{\sum_{k=l}^{m} \sum_{j=1}^{N} P_{G,j}^k} \tag{5.1}$$

$$K_i^{l,m} = c_i^{l,m} \cdot \lambda_u \tag{5.2}$$

The data necessary to perform the calculations to find these three factors are available to the TSO and the balance area operator after the closing of the spot market at 18:00 on the day before operation. This data, however, is subject to forecast errors by the balancing areas[3] and does not include the so called intra-day trading which occurs during the day of operation.

5.2 Scaling λ_u with Generation

The method presented above uses λ_u given by ENTSO-E, which remains constant for at least one year before being updated. From the measurements performed by [25] and [26] it is evident, however, that λ_u has an approximately linear dependency on the total generation active in the system. Therefore an improvement on calculating K_i by simply updating c_i as

[3]Every control area typically managed by a Transmission System Operator (TSO) is made up of multiple balancing areas managed by electric utility companies.

shown in equation (5.2) is to also scale λ_u with the total load in the system at any point in time. In order to do this, λ_u has to be divided by the average load of the year that was used as a base for its original calculation $P_{G,base}$ and multiplied by the average load forecasted for the interval in question. Using the nomenclature introduced above, this is demonstrated in equation (5.3).

$$\lambda_u^{l,m} = \frac{\sum_{k=l}^{m} \sum_{j=1}^{N} P_{G,j}^k}{(m-l+1)} \cdot \frac{\lambda_u}{P_{G,base}} \tag{5.3}$$

Combining equation (5.1) and equation (5.3) into equation (5.4) results in an updated $K_i^{l,m}$ for the hours l to m.

$$K_i^{l,m} = \frac{\sum_{k=l}^{m} P_{G,i}^k}{(m-l+1)P_{base}} \cdot \lambda_u \tag{5.4}$$

This method eliminates the need for the generation forecasts of all areas except for area i itself. This significantly reduces the sensitivity to forecast errors and also eliminates other risks associated with international forecast exchange, i.a. miscommunications, strategic misinformation.

As an effect of the deregulation of electricity markets, some TSOs, such as swissgrid, do not have full access to all generation and load data of their balancing areas. Instead they forecast and measure the "vertical load", which corresponds to the total flow of electric power from the transmission system level to all lower levels. In addition, they also forecast the tie-line powerflows to other areas on the transmission system level. Despite the fact that generators which are connected to a lower voltage level can cancel loads in the lower levels and therefore do not appear in the vertical load, an approximate value for the generation of such an area could be found by adding the vertical load to the net powerflow to adjacent areas. Since no research on the correlation of vertical load and frequency response characteristics exists to date, this approach has to be evaluated in detail before its implementation.

5.3 Construction of β_i by Parts

Instead of relying on RGCE's annually calculated λ_u, which is commonly based on two year old measurements and yearly averages, an algorithm to construct β_i from its four parts can be found by applying the formula given in the OpHB, explained in detail in section 3.2.2, on a much shorter interval and for only one area instead of the entire synchronous grid.

5.3.1 Using Default Values

The specific values given for Primary Control, load self-regulation effect and surplus generation in the OpHB formulas stem from the research and

operating experience of the entire RGCE grid. Using these values for the calculation of the frequency response characteristic of a single area should therefore only serve as a default value if more detailed analyses do not exist. The adaptation of equation (3.21) to (3.24) to a single area i for the hours l to m of one day, as shown in equation (5.5) to (5.8), requires the hourly values of the area's forecasted load $P^k_{load,i}$ and generation $P^k_{gen,i}$ as well as the area's Primary Control reserve $P^k_{prim,i}$ and results in $K^{l,m}_i$ according to equation (5.9).

$$\frac{1}{S^{l,m}_{prim,i}} = \frac{\sum_{k=l}^{m} P^k_{prim,i}}{(m-l+1)\cdot 200\,\mathrm{mHz}} \tag{5.5}$$

$$D^{l,m}_{l,i} = 1\,\frac{\%}{\mathrm{Hz}} \cdot \frac{\sum_{k=l}^{m} P^k_{load,i}}{m-l+1} \tag{5.6}$$

$$\frac{1}{S^{l,m}_{additional,i}} = 0.30 \cdot \frac{1}{S^{l,m}_{prim,i}} \tag{5.7}$$

$$\frac{1}{S^{l,m}_{surplus,i}} = 1\frac{\%}{\mathrm{Hz}} \cdot \frac{\sum_{k=l}^{m} P^k_{gen}}{m-l+1} \tag{5.8}$$

$$\begin{aligned} K^{l,m}_i &= \frac{1}{S^{l,m}_{prim,i}} + D^{l,m}_{l,i} + \frac{1}{S^{l,m}_{additional,i}} + \frac{1}{S^{l,m}_{surplus,i}} \\ &= \frac{1}{m-l+1}(1.3 \cdot \sum_{k=l}^{m} \frac{P^k_{prim,i}}{200\,\mathrm{mHz}} \\ &\quad + 1\frac{\%}{\mathrm{Hz}} \cdot \sum_{k=l}^{m}(P^k_{load} + P^k_{gen})) \end{aligned} \tag{5.9}$$

To improve on this adaptation, the specifics of area i have to be taken into consideration for all four contributing effects. In addition, non-linearities of the frequency response characteristic can be incorporated into a frequency-dependent bias factor $K_i(f)$.

5.3.2 Predicting Primary Control

Calculating Primary Control according to equation (5.5) assumes that the activation of Primary Control occurs linearly in a way that releases the full reserves over the specified band of 200 mHz. However, research presented in section 4.1.3 showed that all generators have an activation deadband which gives rise to a non-linearity in the vicinity of the steady-state frequency. Additionally, the OpHB specification of speed droop control, as summarized in section 2.4, gives rise to a second non-linearity by dictating that the maximum Primary Control has to be released at ±200 mHz. A more realistic, step-wise linear speed droop $S_j(f)$ for a generator j integrating these two

factors, is presented in figure 5.1 and equation (5.10).

$$S_j(f) = \begin{cases} P_{min,j}, & f < f_{min,j}; \\ \frac{P_{min,j}}{f_{min,j}-f_{N-,j}}(f - f_{N-,j}), & f_{min,j} < f < f_{N-,j}; \\ 0, & f_{N-,j} < f < f_{N+,j}; \\ \frac{P_{max,j}}{f_{max,j}-f_{N+,j}}(f - f_{N+,j}), & f_{max,j} > f > f_{N+,j}; \\ P_{max,j}, & f > f_{max,j} \end{cases} \tag{5.10}$$

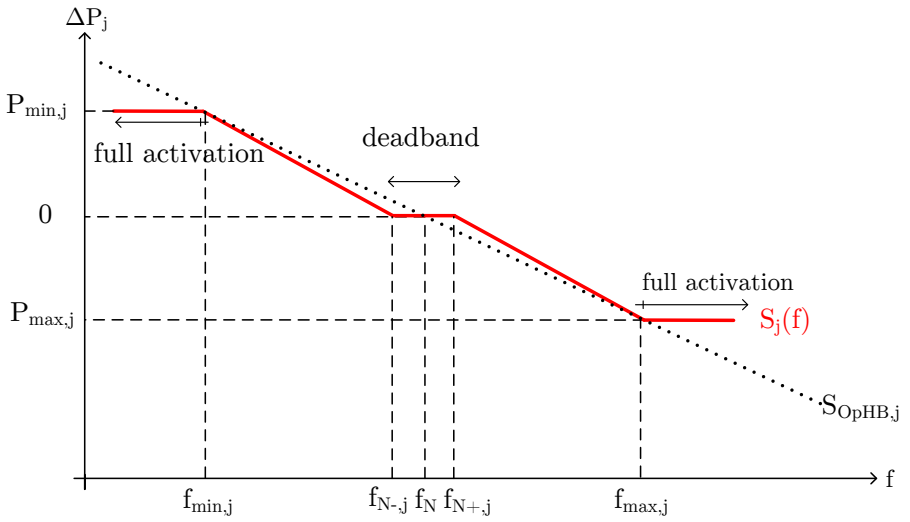

Figure 5.1: Non-linear Speed Droop Model $S_j(f)$ of One Generator compared to the Assumption of OpHB $S_{OpHB,j}$. $f_{N+,j}$ and $f_{N-,j}$ Denote the Deadband Frequencies; $f_{max,j}$ and $f_{min,j}$ Are the Maximum and Minimum Frequencies where Full Activation of Primary Control Reserves Occurs.

The deadband frequencies $f_{N+,j}$ and $f_{N-,j}$ of most generators participating in Primary Control in Switzerland are known from prequalification tests according to swissgrid's specification [32]. The full activation frequencies $f_{max,j}$ and $f_{min,j}$ can be assumed to be $\pm 200\,\text{mHz}$ as specified in the OpHB if more accurate values are not known; $P_{max,j}$ and $P_{min,j}$ are determined regularly by auction.
This model neglects the machine-specific non-linearities occurring between the frequencies $f_{N+,j}$ and $f_{max,j}$ as well as between $f_{N-,j}$ and $f_{min,j}$. These non-linearities are currently not measured during prequalification[4] and thus not usable in the modeling.

[4]If detailed $S_j(f)$ curves were available from other sources such as the manufacturer of the turbine-controller assembly or other test, they could be used instead of the model from figure 5.1

The sum of the inverse of $S_j(f)$ of all generators j participating in Primary Control results in an improved term $\frac{1}{S_{prim,i}(f)}$ according to equation (5.11).

$$\frac{1}{S_{prim,i}(f)} = \sum_j \frac{1}{S_j(f)} \tag{5.11}$$

5.3.3 Additional Primary Control

Equation (5.7) adds 30% additional Primary Control to the simple formula of (Minimal Reserves)/(200 mHz). As explained in section (3.2.2), the causes of this effect are not well documented. For an area i to improve on OpHB's empirical value of 30 %, knowledge of the speed droop controllers present in the system, as well as detailed measurements of their behavior are needed.
A non-linear factor for additional Primary Control could prove to be beneficial, especially when accounting for generators which do not officially take part in the auctioned Primary Control. According to swissgrid, many generator operators decide to widen the deadbands of the speed droop controllers, instead of switching them off completely, in order to help sustain the frequency in cases of large deviations.
Until reliable data in the area of additional Primary Control exists, the RGCE's default value of 30% has to be used to calculate any area's K_i factor.

5.3.4 Measuring Surplus Generation

Surplus generation is explained in the OpHB to originate from the speed droop of (100%)/(50 Hz), which approximately 50% of all generators exhibit. It is clear that large generators employing sophisticated speed droop controllers count towards the other half of all generators, not included in surplus generation.
The constant surplus generation factor of 1 %/Hz takes into account only the size of the generation in the RGCE grid, which is then split amongst its areas by the contribution factor c_i. It is reasonable to assume, however, that the different types of power plants have different influences the overall 1 %/Hz surplus Generation. It is further safe to assume that Switzerland's fraction of the surplus generation does not correlate with its contribution factor c_i because the types of power plants prevalent in Switzerland are not proportional to those of the entire RGCE. This fact is illustrated in table 5.1 which compares the sources of primary energy converted to electricity in 2009. A further complication comes with the time-dependence of these shares. Switzerland in particular sees large changes in its hydro power plant activity in correlation with the seasons and the electricity market prices. As with additional Primary Control, because of the lack of research, there exists no support for a value other than the OpHB's default for surplus generation.

Type of primary power	Switzerland	RGCE
Nuclear	39.3 %	28.8 %
Fossil	3.1 %	51.1 %
Hydro	55.9 %	12.6 %
Other renewables	0.2%	6.9%

Table 5.1: Share of Different Power Plants on the Annual Electricity Generation in 2009, Data from [5].

5.3.5 Load Self-Regulation

As discussed in section 4.1.5, the load self-regulation factor of 0.5 %/% specified by the OpHB is not beyond doubt. Welfonder et al., [29] and [30], showed that on average between 1989 and 1991, the load self-regulation effect measured at seven different points in Germany came to be 1.5 %/%. However, seasonalities on average showed values 20 % higher in summer and 20 % lower in winter. In addition, intra-day variations of +11 % during office-hours, -2 % during night-time and -8 % during evening-hours and weekends were found.

For the lack of more current measurements, and more importantly measurements performed in Switzerland, the results found by Welfonder et al. can be used as a basis when constructing β_i by parts. The author thus proposes the following algorithm derived directly from the results of [29] to calculate the load self-regulation factor $D_{l,i}^{k,n}$ for the hour k on day n of the week:
The base value $D_{l,i}^{base}$, is set to 1.8 %/% for May-September and to 1.2 %/% during October-April. In order to account for changes during the hours of the day and days of the week, a factor $\gamma_i^{k,n}$, defined in equation (5.12), can be used to determine $D_{l,i}^{k,n}$ according to equation (5.13).

$$\gamma_i^{k,n} = \begin{cases} 1.11, & 0 \leq n \leq 5 \wedge 6 \leq k < 18; \\ 0.92, & 6 \leq n \leq 7 \wedge 6 \leq k < 18; \\ 0.92, & 0 \leq k < 6; \\ 0.98, & 18 \leq k < 0 \end{cases} \tag{5.12}$$

$$D_{l,i}^{k,n} = \gamma_i^{k,n} \cdot D_{l,i}^{base} \tag{5.13}$$

5.3.6 Sensitivity to Parameter-Changes

When constructing λ_i as specified by the OpHB, the aforementioned four parts contribute different shares as shown in table 5.2. In addition, these parts also depend on different quantities of the power system, namely the load, generation and Primary Control present in the area i. It is clear from table 5.2 that the mandatory 3000 MW of Primary Control which have to

be delivered over 200 mHz, account for the largest share of the Frequency Response Characteristic. Furthermore, additional primary control is directly proportional to the Primary Control, resulting in an overall 73.1 % of λ_i being made up of Primary Control. Changing the calculation of Primary Control, as suggested in section 5.3.2, thus has significant impact on the size and frequency-dependancy of λ_i.

Cause	Absolute Value $[\frac{\text{MW}}{\text{Hz}}]$	Relative Value [%]	Dependency
Primary Control	15000	56.2	–
additional Primary Control	4500	16.9	Primary Control
surplus generation	3060	11.5	Generation
Load Self-Regulation	4120	15.4	Load

Table 5.2: Analysis of the Four Parts of λ_u according to the OpHB.

The two remaining parts each make up considerably smaller shares of 11.5 % and 15.4 % of the total λ_i, however, they depend on the generation and the load present in the system, which vary considerably over time. Detailed load data[5] of Switzerland evaluated for 2010 shows a minimum value of 5016 MW at 04:00 on August 18th and a maximum of 10835 MW at 18:00 on December 15th. Assuming that the generation varies similarly, it has to be considered that surplus generation and load self-regulation, which combined make up 26.9 % of λ_i by OpHB calculations, can deviate by as much as 100 % when using the algorithms proposed in section 5.3.4 and 5.3.5.

Furthermore, the load self-regulation effect's share of the total frequency response characteristic of 15.4 % increases to between 17.0 % and 30.9 % when using the algorithm from section 5.3.5 instead of the constant factor of 1 %/%.

It is clear from these calculations that the major influence on recalculating λ_i with the algorithms described previously is the modeling of Primary Control. However, the quality of forecasts concerning load and generation as well as the load self-regulation factor $D_{l,i}$ also carry considerable significance.

5.4 Measuring β_i

Predicting β_i by using calculations such as the ones presented above, has proven to be challenging for different reasons, the most important being the lack of research in the area. Another major obstacle is the difficulty of measuring the actual frequency response characteristic β_i of an area i in order to verify the accuracy of the calculation of the frequency bias factor K_i

[5]ENTSO-E's data portal [33] releases hourly measured load for every third Wednesday of every month for every area in the RGCE.

have to be investigated. Measurements recorded during outages have served as guidelines and as benchmarks for the calculations in the past but they have never been used to directly update K_i factors in areas of the RGCE.

5.4.1 Analysis of Large Outages

Traditionally large outages, which were either induced deliberately or occurred by accident, were used to measure β of a synchronous area according to equation (2.13) by dividing the size of the outage by the frequency deviation it caused. For this purpose, the OpHB obligates the members of the RGCE to record data concerning every outage of more than 600 MW.

For the calculation of β_i of an individual control area i within the synchronous area, two cases have to be considered. Either a disturbance happens in an area $k \neq i$ or it occurs inside the area i itself. In the first case, the change in exported power immediately following the change in frequency is composed of area i's Primary Control, Load Self-Regulation and Surplus Control and is thus proportional to β_i as shown in equation (5.14). The latter case triggers support from all areas $k \neq i$, which results in an import of supporting power proportional to the load frequency response characteristic of all areas except area i according to equation (5.15). In both cases, the frequency deviation and the change in exported power resulting from the outage have to be evaluated at a point in time shortly after the outage, when Secondary Frequency Control loops are not yet active.

$$\beta_i = -\frac{\Delta P_{T,i}(t_{0^+})}{\Delta f(t_{0^+})} \tag{5.14}$$

$$\beta - \beta_i = \frac{\Delta P_{T,i}(t_{0^+})}{\Delta f(t_{0^+})} \tag{5.15}$$

The events leading to these large disturbances occur only seldomly and at random times. They are therefore not appropriate as a sole method of determining the frequency bias factor of Secondary Control. Large outages can, however, serve as an evaluation and correction method for an algorithm which predicts β_i.

5.4.2 Linearity in Random Disturbances

Unlike the large disturbances treated in the previous section, small, random mismatches between the mechanical power fed into generators and the electric power consumed by the sum of all loads in a grid happen constantly in all areas. Each small disturbance only produces a minor frequency deviation but summed over the total of the RGCE they can lead to considerable changes in the system frequency at any given point in time.
The constant presence of these random disturbances provides a viable base

for constant benchmarking of β_i calculation methods and potentially for an automatted error correction algorithm.

For a small area i, such as Switzerland, which makes up only between 2 % and 3.5 % of the total generation of the synchronous area at any time, the vast majority of random disturbances take place in other areas $j \in \Omega_i$. Therefore, the frequency deviations resulting from the sum of these disturbances can be treated similarly to the ones resulting from large outages. Unlike large disturbances, however, the exact size of the mismatch in mechanical power produced and electrical power consumed is not known. Thus, an algorithm for the calculation of β_i other than equation (5.14) has to be derived.

$$\Omega_i = \{1, \ldots, N\} \backslash \{i\} \tag{5.16}$$

As explained in chapters 2 and 3, the initial change in exported power $\Delta P_{T,i}^{t_{0+}}$ of an area i to a frequency deviation Δf is directly proportional to that area's frequency response characteristic, as shown in equation (5.17). Shortly after the initial response, the Secondary Control loop will activate Secondary Control power $\Delta P_{AGC,i}$ according to equation (3.1) which is also exported to the areas Ω_i causing the disturbances, resulting in the exported power given in equation (5.18). If this area's K_i is set to be exactly equal to its β_i, the area control error ACE_i stays equal to 0 MW over the course of the frequency disturbance according to equation (3.12). As a result, area i does not activate Secondary Frequency Control and thus exhibits a deviation in export power linear to β_i.
The research presented in chapter 4 and an analysis of swissgrid's ACE data, however, suggests that K_i differs from β_i during normal operation.
Assuming an K_i to be the actual β_i plus an error factor e_i as shown in equation (5.19), ACE_i from equation (3.12) can be written according to equation (5.20). Inserting this into equation (3.1) yields $\Delta P_{AGC,i}(t)$ as a function of $\Delta f(t)$ and of its own integration, as seen in equation (5.21). Finally, inserting equation (5.21) into equation (5.17), gives the deviation of export power as a function of $\Delta f(t)$ and the Secondary Control energy exported during the deviation as shown in equation (5.22). In most literature, Δf is suggested to be directly influenced by $\Delta P_{T,j}$ of any area j. However, for areas i of very small size, the effect of $\Delta P_{T,i}$ on the frequency deviation of the entire interconnection can turn out to be almost negligeable. This allows for the analysis of $\Delta P_{T,i}$ as a function of Δf.

$$\Delta P_{T,i}^{t_0+} = -\beta_i \cdot \Delta f \tag{5.17}$$

$$\Delta P_{T,i}(t) = -\beta_i \cdot \Delta f(t) + \Delta P_{AGC,i}(t) \tag{5.18}$$

$$K_i = (1 + e_i) \cdot \beta_i \tag{5.19}$$

$$ACE_i(t) = e_i\beta_i \cdot \Delta f(t) + \Delta P_{AGC,i}(t) \tag{5.20}$$

$$\begin{aligned}\Delta P_{AGC,i}(t) = & -\frac{C_{p,i}e_i}{1+C_{p,i}}\beta_i\Delta f(t) - \frac{1}{T_{N,i}(1+C_{p,i})} \\ & \cdot \int \left(e_i\beta_i\Delta f(t) + \Delta P_{AGC,i}(t)\right) dt\end{aligned} \tag{5.21}$$

$$\begin{aligned}\Delta P_{T,i}(t) = & -\left(\frac{C_{p,i}e_i}{1+C_{p,i}} + 1\right)\beta_i\Delta f(t) - \frac{1}{T_{N,i}(1+C_{p,i})} \\ & \cdot \left(\int e_i\beta_i\Delta f(t)dt + \int \Delta P_{AGC,i}(t)dt\right)\end{aligned} \tag{5.22}$$

For the error factor e_i, two cases have to be distinguished: Either $K_i > \beta_i$, leading to a positive e_i or $K_i < \beta_i$, resulting in a negative e_i. As discussed in section 4.2, the first case will lead to Secondary Control power which supports the activated Primary Control power, while the latter leads to an opposite reaction of the Secondary Controller, which will lead to a partial cancellation of the Primary Control power within the area i itself.

It is clear from equation (5.22) that for small error factors e_i, the deviation in export power scales almost linearly with the frequency deviation $\Delta f(t)$ for any point t in time. In cases of large differences between K_i and β_i, the time dependent integrals will reduce the effect of the linear relation between $\Delta f(t)$ and $\Delta P_{T,i}$. The effects of the sign of e_i and the non-linearities on $\Delta P_{T,i}$ as a function of Δf are shown in figure 5.2.

In addition to the non-linearity introduced by e_i, pre-disturbance offsets in $\Delta P_{T,i}$ lead to additional noise. Especially in small areas, it is possible that tie-line power flows occur without a resulting change in system frequency if the power flows are compensated by another area; in figure 5.2 these offsets can lead to $\Delta P_{T,i}(\Delta f)$ curves which are vertically displaced.

As a sizing method for K_i, the continuous analysis of $\Delta P_{T,i}$ as a function of Δf could provide advantages over the current method of applying static formulas to system properties such as load and generation volumes. In order to implement such a method, sophisticated stochastic algorithms, as well as artifical intelligence strategies that couple $\Delta P_{T,i}$ and Δf to important power system properties such as seasonality, weather-effects and load-schedules, have to be devised. This was deemed outside the scope of this project and thus remains as a future research possibility for interested parties.

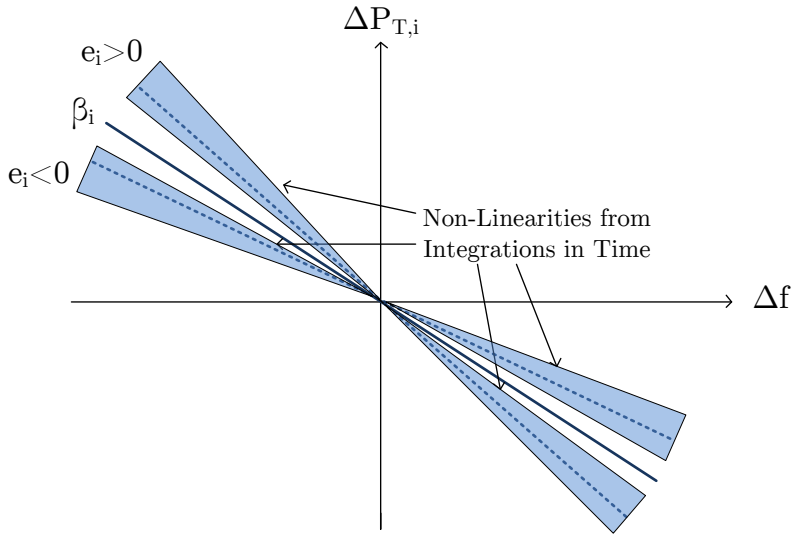

Figure 5.2: Deviation in Export Power Flow as a Function of the Frequency Deviation. The error factor e_i changes the Slope and Introduces Non-Linear Effects.

Chapter 6

Calculation, Modeling and Simulation

In order to compare the performance of the different sizing methods for K_i proposed in sections 5.1 to 5.3, a simple, semi-dynamic frequency control simulation in Matlab/Simulink was derived. The model was to be set according to specific load- and generation scenarios at which β and β_i were known.

6.1 Reduced-Size Power System Model

To simulate the behavior of an AGC employing different K_i factors, a power system model of small size was created, closely following the models presented in [2]. Since short-term phenomena, such as power plant dynamics and small-signal frequency swings are not of importance for AGC, as pointed out in [8], the modeled power system shares one common frequency and employs only first-order delays as power plant models.

For the simulation, the synchronous grid of the RGCE is divided into three different areas. The updating algorithms for the K_i factor are implemented in the AGC of area one. The second area designates the control area which sustains a step-wise discrepancy between its mechanical and its electrical power (i.e. an outage of generation or load) and the remainder of the RGCE load and generation is concentrated in the third area. The simulation is designed to only calculate deviations from normal operation values, such as frequency (Δf) and tie-line power flows ($\Delta P_{T,i}$). The pre-disturbance properties of the power system are used to determine influences, namely the frequency response characteristics of the individual areas.

Partitioning the synchronous grid in such a way enables the simulation of the reaction of the AGC in the first area to an outside outage, while incorporating all of the load and generation present in the entire grid at the time of the incident. The ideal outcome for a K_i-factor calculation would

be to have an exact match with β_i. In the simulation, this would equate to a complete lack of reaction of the AGC in area one to a disturbance in area two.

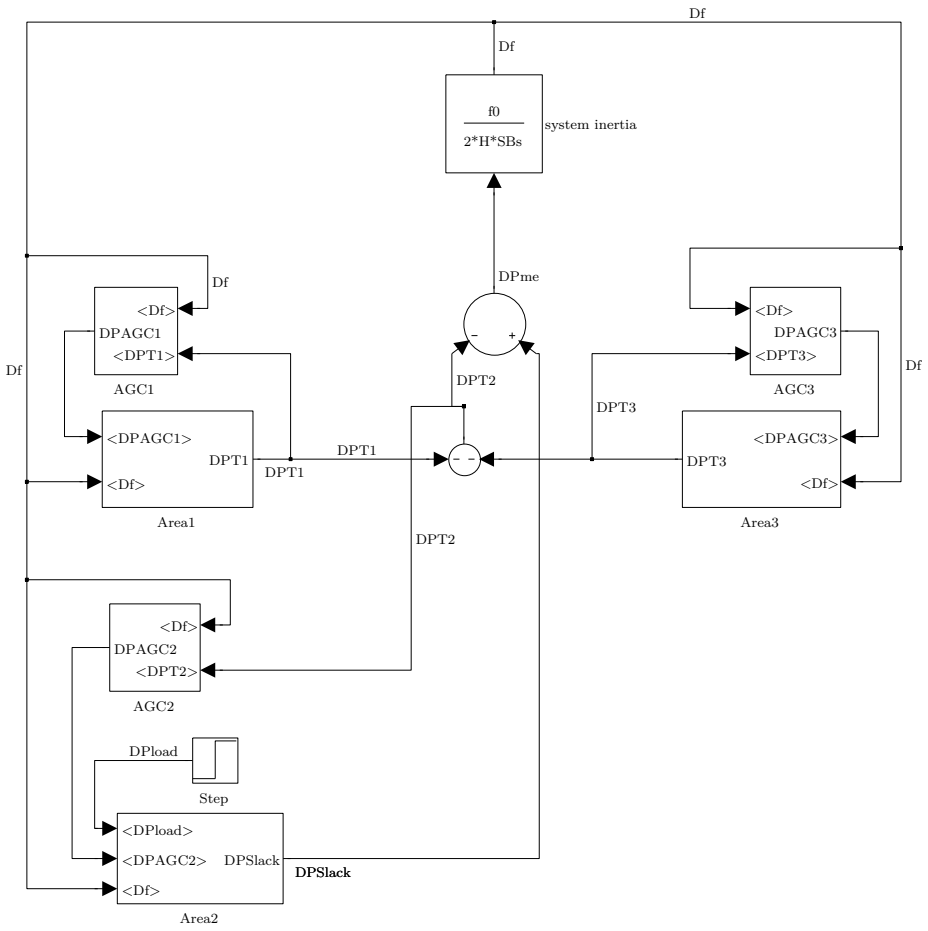

Figure 6.1: Reduced-Size Model of the RGCE Synchronous Area in Simulink.

Figure 6.1 shows the top layer of the Simulink model incorporating the three individual areas. The blocks labeled *Area1 − Area3* contain Primary Control as well as the load self-regulation, as seen in figure 6.2 for area three. These blocks also contain a first order delay modeling the Secondary Control power plants. For the second and third area, Primary Control and load self-regulation is assumed to behave linearly according to a β_j which can be specified individually for every simulation.
The blocks *AGC1 − AGC3* contain the Automatic Generation Control of each area, shown in figure 6.3 for area one, which consists of a PI controller and an ACE calculation block depicted in figure 6.4.

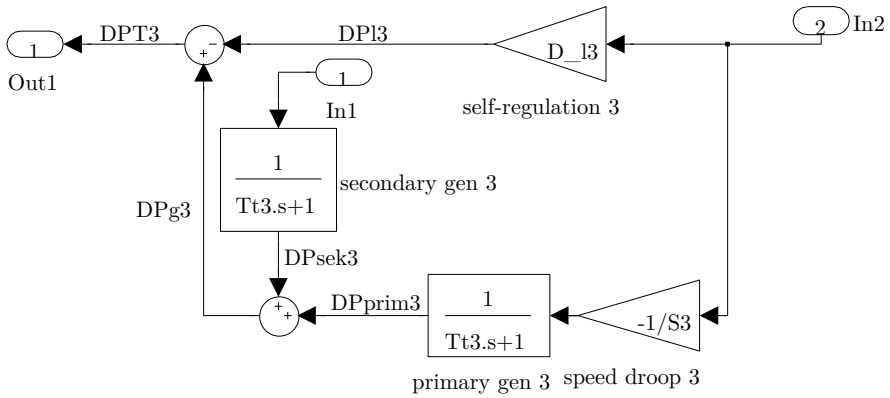

Figure 6.2: Simulink Block of *Area3* Containing Linear Primary Control via Speed Droop and Self Regulation as well as First Order Delays which Model Power Plant Behavior. The Sum of the Change in Generation (Primary and Secondary) is Added to the Change in Load Self-Regulation which Results in a Change in Tie-Line Power Flow *DPT3*.

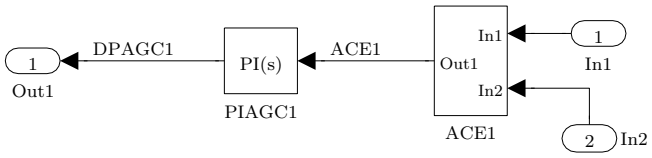

Figure 6.3: Model of the AGC of Area One, Where Inputs *In1* and *In2* Feed Δf and $\Delta P_{t,1}$ into the ACE Calculation Block. The PI controller *PIACG1* Produces the Control Signal *DPAGC1* for the Secondary Control Plants.

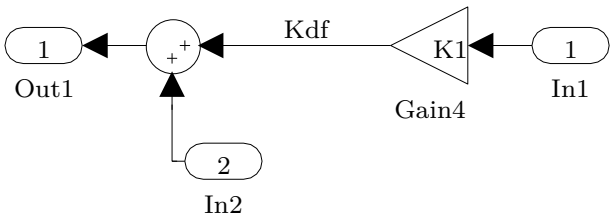

Figure 6.4: Calculation of the Area Control Error of Area One with a Linear Frequency Bias Factor K_1.

6.1.1 Power System Dynamics and Tie-Line Flows

As seen in figure 6.1, the system frequency deviation is computed as a result of one single system inertia block. This block incorporates the sum of all inertial constants and generator ratings of the synchornous area as to generate only one shared frequency deviation. The mismatch between electrical and mechanical power, which defines the input of the system inertia block, is calculated as the difference of the power of the outage in area two and the sum of the frequency dependent power change in all areas.

In the same way, the tie-line power flows from areas one and three to the area in need are simply calculated as the sum of the frequency dependent power production and consumption in areas one and three. This calculation assumes that during the outage in area two, no other outages or similar phenomena occur.

6.1.2 Primary and Secondary Control

For area one, Primary Control was modeled as four different generators with individual, non-linear speed droops $S(\Delta f)$, presented in figure 6.5. Generators one, two and three each account for approximately one third of the Primary Control reserves allocated to Switzerland over a band of 200 mHz; the fourth generator is included to model additional Primary Control. All speed droops feature deadbands of different sizes around $\Delta f = 0$ as well as specific frequencies at which their control reserves are fully activated. Additionally, generator three contains a continuous non-linearity in the form of a square-root function. The resulting speed droop of the sum of these four generators is shown to differ from the classic assumption of linear $S(\Delta f)$, especially for small and for large variations in frequency.

For simplicity and because their behavior is not significant for the performance of AGC in area one, Primary Control in areas two and three area assumed to be linear speed droop controlled power plants with low first-order delays as seen in figure 6.2.

6.2 Implementation of K_i-factor Algorithms

6.2.1 OpHB Definition

In order to have a baseline for measuring any improvement, K_i of Switzerland as well as the Primary Control reserves and the λ_u of the RGCE were taken directly from the instruction of the UCTE or ENTSO-E, depending on the simulated year.

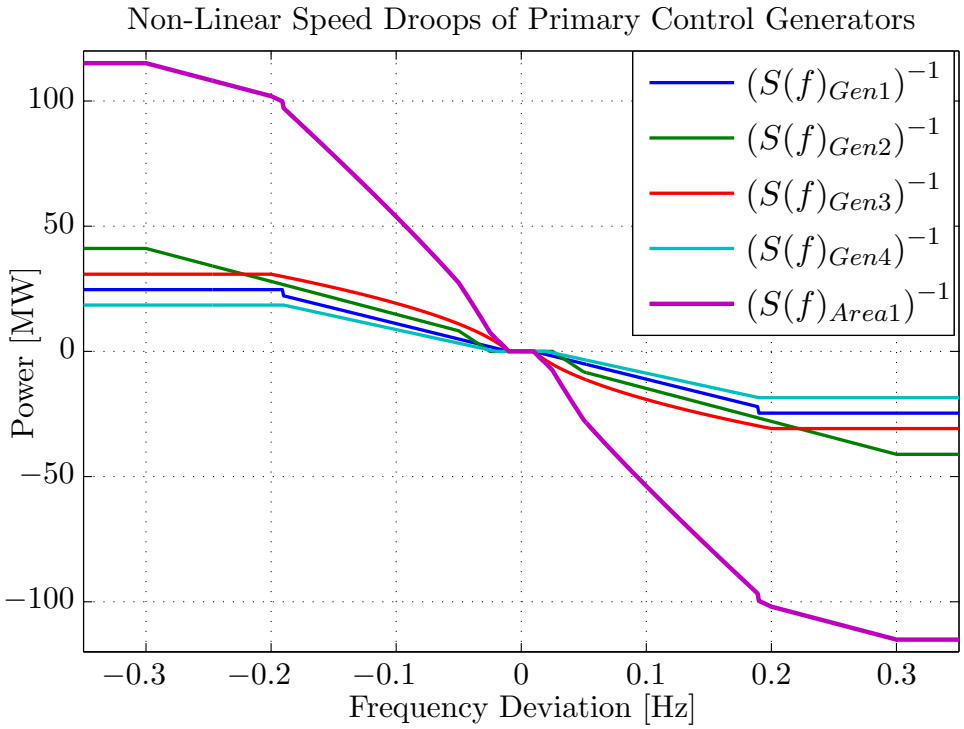

Figure 6.5: Non-Linear Speed Droops of Primary Control Power Plants of Area One.

6.2.2 Updating c_i and scaling λ_u

The algorithms described in sections 5.1 and 5.2 were implemented in the simulation for time intervals of 0:00-8:00, 8:00-20:00 and 20:00-0:00. The generation during these time intervals was calculated by adding every area's export powerflow to its load because detailed generation data is not made available through the ENTSO-E.

6.2.3 Simple Partwise Construction

"Simple partwise construction" refers to the calculations presented in section 5.3.1. It involves applying the definition of λ_u to a single area on the same time-intervals used for the calculations of c_i and λ_u above.

6.2.4 Non-Linear partwise $K_i(f)$

The fourth algorithm proposed in section 5.3.2 differs from the simple partwise construction by taking into account more accurate load self-regulation measurements and non-linear Primary Control speed droops. For the latter, it is assumed that the specifics of the deadbands and the full activations are known for Primary Control generators one, two and three. The fourth generator accounts for the additional Primary Control and cannot be predicted when setting $K_i(f)$.
In order to realize a frequency dependent $K_i(f)$, the calculation of the ACE shown in figure 6.4 was changed to figure 6.6, where a Matlab function replaces the previously linear multiplication.

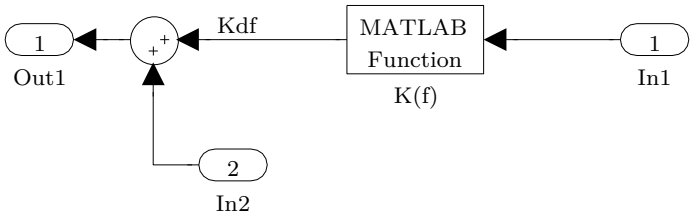

Figure 6.6: Calculation of ACE_1 for a Non-Linear $K_i(f)$, Using a Frequency Dependent Matlab Function.

6.3 Evaluation Result Output

For every one of the four proposed sizing methods as well as the standard OpHB values, the simulation program plots the time-domain behavior of important system variables. Additionally various indicators of Secondary Control quality introduced in chapters 2 and 4 are compared amongst the

different sizing methods. In the examples below, the information in the different plots is explained; the corresponding figures can be found in appendix A.

Time-domain performance of characteristic values of area one is shown in figures 6.7, A.1 and A.2. These figures are generated separately for every sizing method. The first two show the frequency-dependent change in generation and in load in area one and the resulting change in tie-line powerflow. The last figure shows the input, internal states and output of the AGC over time, which can be helpful in reconstructing the area's response in Secondary Control power.

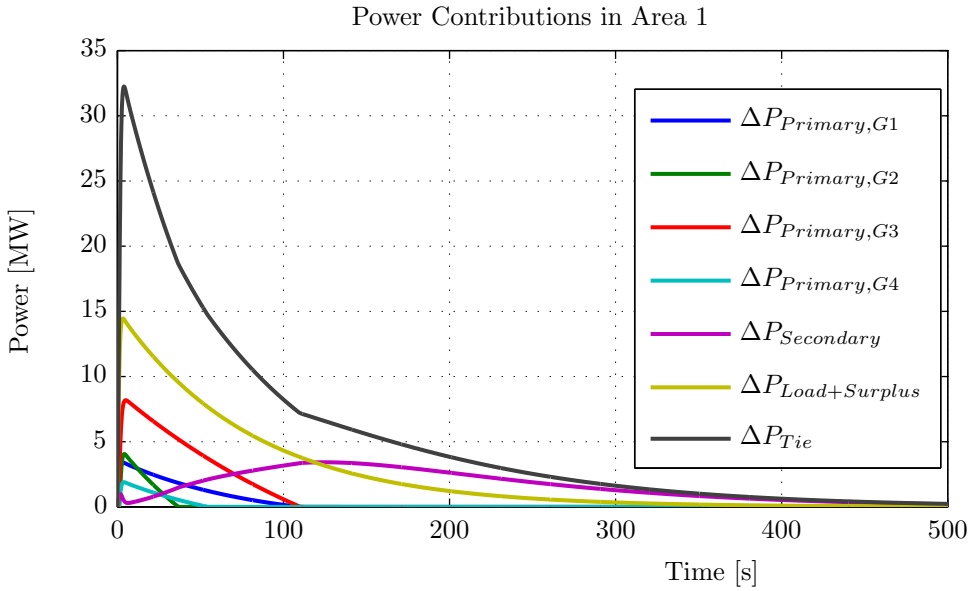

Figure 6.7: Share of the Primary and Secondary Control Power and Load Self-Regulation of the Tie-Line Power over Time.

Development of the total power generation and consumption is split up into its sources in the different areas in figure 6.8. The ACE and $\Delta P_{AGC,i}$ of the AGCs of all areas are presented in figure A.3. Both figures can help in analyzing the interaction of the different frequency dependencies and the performance of the AGCs in all three areas.

Comparisons of the effect of the different K_i-factor calculation methods are shown in figures 6.9 through A.6. The different $K_i(\Delta f)$ calculated are displayed in figure A.6. Figures 6.9 and A.4 compare the operation of the AGC in the first area; the non-linearites in the calculated ACE originate from the non-linear Primary Control generator models. The plot of the change in tie-line powerflow for the different sizing methods

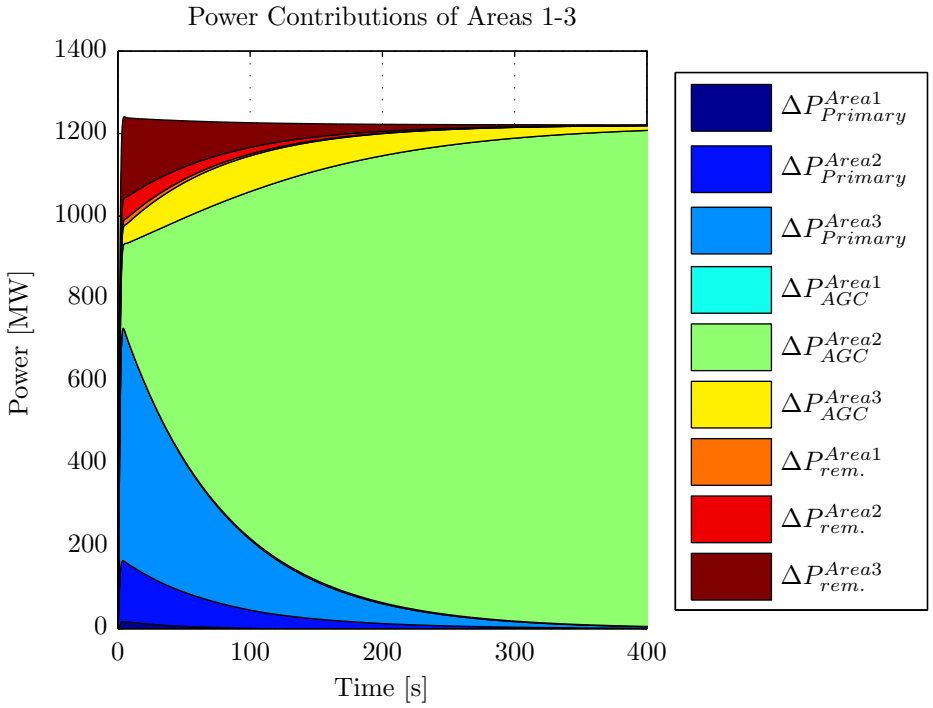

Figure 6.8: Share of All Areas' Frequency Dependent Generation and Load of the Total Change in Power.

in figure A.5 has to be analyzed carefully because while lower values of ΔP_{Tie}^{Area1} indicate lower congestion, they can also indicate a cancellation of Primary Control power by interfering Secondary Control.

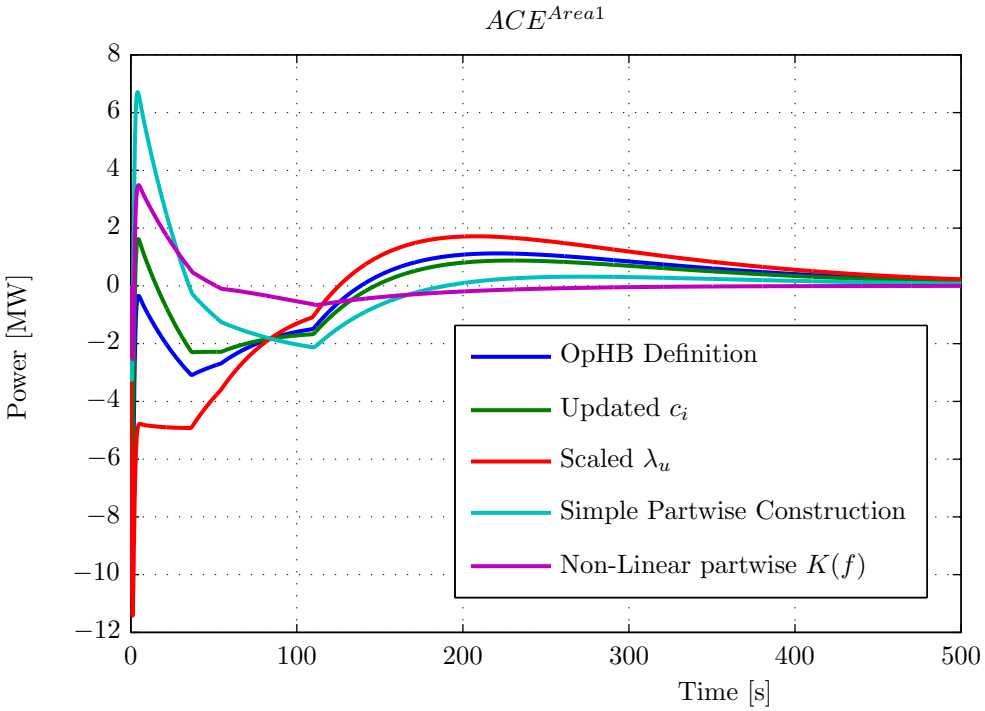

Figure 6.9: Area Control Errors of the First Area's AGC for the Different K_i Calculation Algorithms.

The summary of the performance of the different K_i-factor calculation methods is generated in the form of a spider plot, as seen in figure 6.10. The size of the area spanned in the spider plot is inversely proportional to the performance of the corresponding algorithm. Interfering and supporting AGC power and energy is calculated according to equations (4.2) and (4.3). These values serve as an indication of how much Secondary Control power was triggered as a result of the disturbance. The maximum value of the ACE and its integration over time are measurements for the mismatch between the area's actual β_i and the AGC's K_i.

6.4 Input Data

In order to simulate the influence of different K_i calculation algorithms, the most important system properties, as listed below, have to be known for the

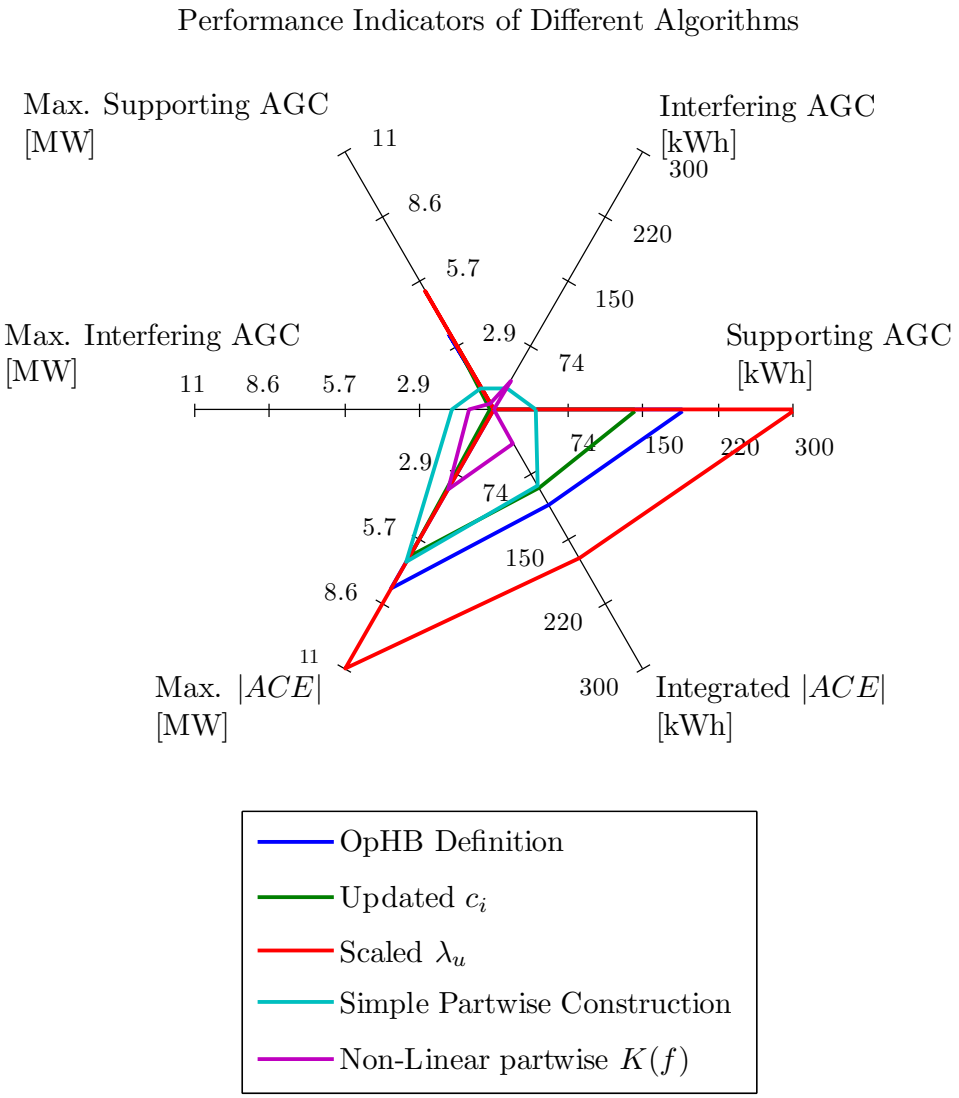

Figure 6.10: Spider Plot Comparing the Most Important Performance Indicators of the Different $K_i(f)$ Calculation Algorithms. Smaller Area Correlates to Better Performance.

specific point in time.

β and β_i at the specific time, in order to compare the calculated K_i to the actual β of the net.

Size of the disturbance in combination with β is used to simulate the initial frequency deviation as explained above.

Load values over the course of the day when the simulation takes place have to be known in order to calculate the load self-regulation effect at the specific time and to calculate K_i.

Net export powerflows are added to the load to give the generation present in every area during the simulation, is needed for the calculation of different K_i-factors.

The load and export powerflows can be obtained through ENTSO-E's data portal [33]. While the load of every area in the RGCE is available as hourly averages for every third Wednesday of the month, only snapshots of the export powerflows at 3:00 and at 11:00 are available on these dates. During normal operation the predictions of load and export powerflows, which would be used to calculate K_i, always contain a forecast error which originates from system variations between days. As a result, the error in the simulation introduced by selecting a weekday reasonably close to the third Wednesday can be treated as forecast error which occurs naturally in the power system. Running the simulation for the load and export powerflow situation on a Saturday or Sunday is not advised since the correlation between the third Wednesday and a weekend day can be far greater than realistic forecast errors.

6.4.1 Large Disturbance

To obtain a direct comparison between the simulation and the response of the real power system, analyses of selected outages performed by swissgrid employing the method presented in section 5.4.1 yielded values for β, β_i and the size of the disturbances, which are listed in table 6.1. It is evident from the table that the frequency response characteristic of the entire network β tends to be higher than the yearly calculated value λ_u. According to the calculations performed in section 4.2, this can result in interfering Secondary Control power being provided in some areas. However, since the exact difference between β and λ_u depends on the time of day and and the season, these measurements lend some credibility to the assumption that β scales with the generation present in the system.

Unlike β, β_i varies widely between the different outages and does not seem to be correlated to the variation of β. To analyze the accuracy of

Date	Country	Size [MW]	β_i $\left[\frac{\text{MW}}{\text{Hz}}\right]$	$\beta_i - K_i$ [%]	β $\left[\frac{\text{MW}}{\text{Hz}}\right]$	$\beta - \lambda_u$ [%]
Tue. 31.07.2010 09:55	France	1294	591	-9.5	29432	10.9
Tue. 17.08.2010 15:23	France	1221	909	39.2	27750	4.6
Wed. 15.12.2010 22:50	Poland	1031	1406	115.3	32219	21.4
Tue. 18.01.2011 17:05	Italy	2250	462	-32.2	34615	31.0

Table 6.1: Details of the Different Outages Analyzed by swissgrid.

the β_i measurements, different plausibility checks were applied to the data depending on the specifics of the supplied data sets. Where available, the ACE generated by swissgrid's AGC was compared to the theoretical values calculable by equations (5.20) and (3.12) when using β_i calculated by swissgrid. In addition, for every data set, the relationship of β_i to the calculations from equation (5.14) was examined.

As an example, figures 6.11 and 6.12 show the frequency and the export power deviations measured by swissgrid between 17:00 and 17:10 on Tuesday, January 18th, 2011. At 17:05:44 the failure of a bus bar in Italy lead to a momentary loss of 2250 MW of generation in the RGCE grid. In figure 6.11

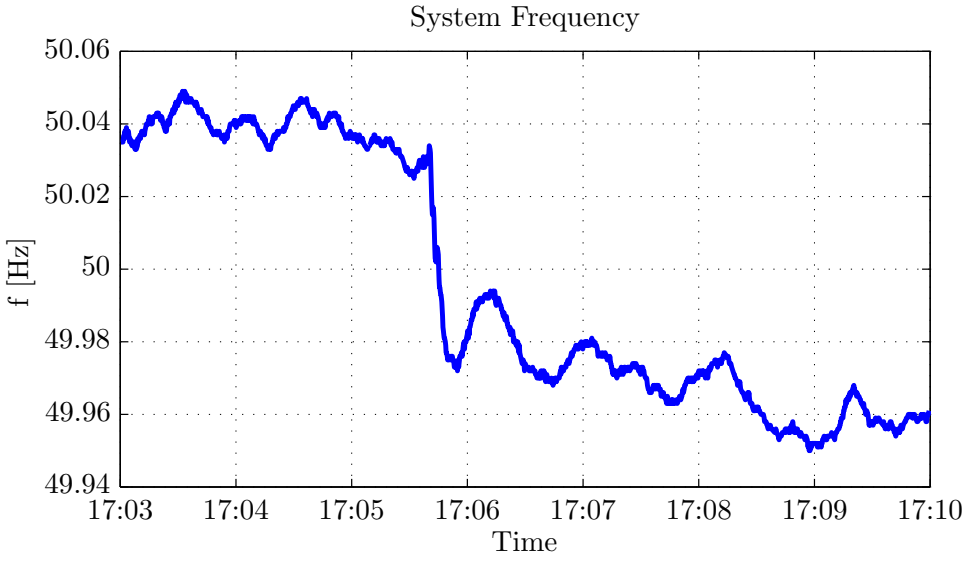

Figure 6.11: System Frequency measured by swissgrid between 17:00 and 17:10 on January 18th 2011. Outage in Italy of 2250 MW generation occurs at 17:05:44.

the system frequency is shown to have dropped rapidly by approximately

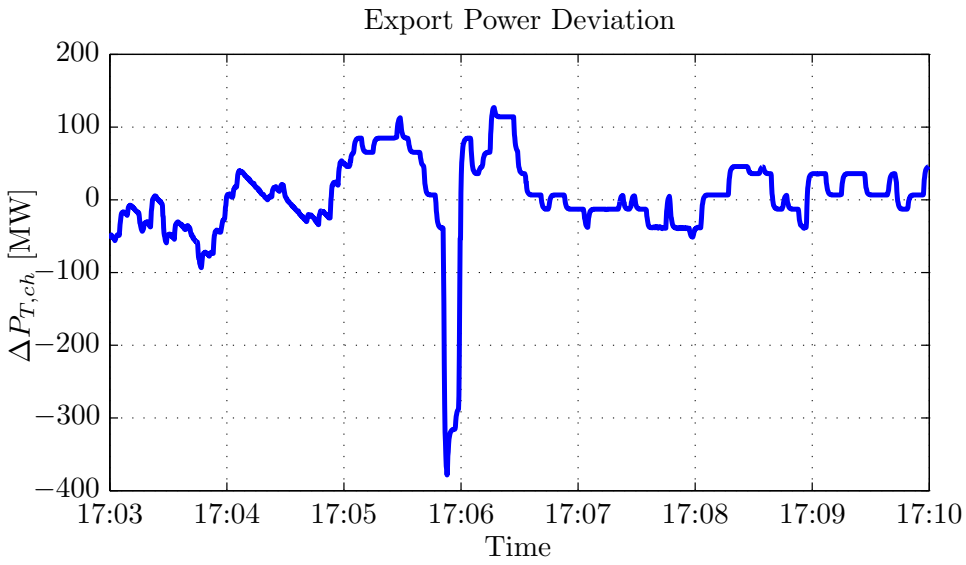

Figure 6.12: Export Power Deviation from Schedule between 17:00 and 17:10 on January 18th 2011. Outage in Italy of 2250 MW Generation Occurs at 17:05:44.

65 mHz, which according to equation (2.13) adds up to a frequency response of the whole grid of 34615 MW/Hz, which is 31 % above the OpHB reference of 26680 MW/Hz. Figure 6.12 shows a decrease in Switzerland's exported power of almost 500 MW during the decrease in frequency, which is not at all consistent with the expected increase of supporting power of about 44 MW according to K_i or the 30 MW according to β_i calculated by swissgrid.

From the results of these plausibility checks it can be concluded that measuring β_i of Switzerland by applying equation (5.14) to large disturbances does not yield realistic results.

It is possible that the data delivered by swissgrid for the four outages was affected by technical failures, such as measurement insensitivities or data storage corruption, however, the most plausible explanation for the phenomenon of widely varying β_i and $\Delta P_{T,i}$ lies in the size of Switzerland's load and generation in comparison to the total size of the synchronous grid, as well as the large capacity of the high voltage lines connecting Switzerland to its neighboring areas. The share of frequency sensitive generation and load in Switzerland is negligible compared to the transit power flows which result from dynamics of large parts of the RGCE grid.
During these large disturbances, a power system of the extent of the RGCE acts very dynamically. In addition to the fact that in most cases, the system was not in a true 50 Hz equilibrium before any of the disturbances; there are a large number of different interactions such as incorrectly configured control loops, protection equipment and unscheduled tie-line flows which can affect the accuracy of the results from equation (5.14) and (5.15). These

dynamics have insignificant effects on the overall β of the whole grid, but for a small area such as Switzerland, they can dominate the natural dynamics and subsequently lead to unusable data.

6.4.2 Random Disturbances

Since the analysis of the large disturbances provided by swissgrid did not yield usable β_i for given points in time, more detailed data was requested in an attempt to apply the methods demonstrated in section 5.4.2. The delivered data contained measurement series of the frequency, ACE, and export powerflow for the same days when the aforementioned outages occurred.

While the findings are consistent over all measurements, the following figures show exemplary data of one hour on Monday, January 17th, 2011 at which the effects presented themselves especially clearly. The first attempt at estimating β_i was to plot the ACE as a function of the frequency deviation in order to find lines with a slope proportional to $e_i\beta_i$ as suggested by equation (5.20). In figure 6.13, there are at least seven lines with approximately the same slope, this slope corresponds exactly to K_i set in the AGC. According to equation (5.20), however, this slope should be equal to the error term e_i multiplied by the frequency response characteristic β_i, which is equal to the difference between K_i and β_i. An analysis of the data points showed that the measurements which appear close together in the same line of the $ACE(\Delta f)$ plot are not all proximate when analyzing the ACE as a function of time, as done in figure 6.14. $ACE(t)$ appears to oscillate with an amplitude of $\pm 50\,\mathrm{MW}$ around $0\,\mathrm{MW}$. The deviation of the frequency from its setpoint, shown in figure 6.15, slowly increases from almost -40 mHz to 50 mHz over the course of the hour, while exhibiting small oscillations in the range of a few millihertz. The slope of K_i in figure 6.13 suggests that the second term in calculating ACE, $\Delta P_{T,i}$, is not frequency dependent. This was analyzed in figure 6.16 for the same interval in time. In this plot, the only discernible lines run parallel to the frequency axis, with a slope of $0\,\mathrm{MW/Hz}$. According to equation (5.22) the only explanation for this phenomenon is that the integration components of the frequency deviation and the AGC power compensate the frequency dependency of the Primary Control. A fundamentally different explanation is to use the same argumentation as for large disturbances, which says that the tie-line powerflow in and out of Switzerland is dictated by neighboring countries and cannot be calculated according to equation (5.18), rendering the basis of the analysis of $\Delta P_{T,i}$ as a function of Δf in order to find β_i irrelevant. Both explanations are supported by figure 6.17, which shows the export powerflow out of Switzerland over time. If the powerflow were proportional to the frequency deviation in some way, $\Delta P_{T,i}$ would show a noticeable difference between the first half and the second half of the hour as the frequency deviation changes signs around 23:30.

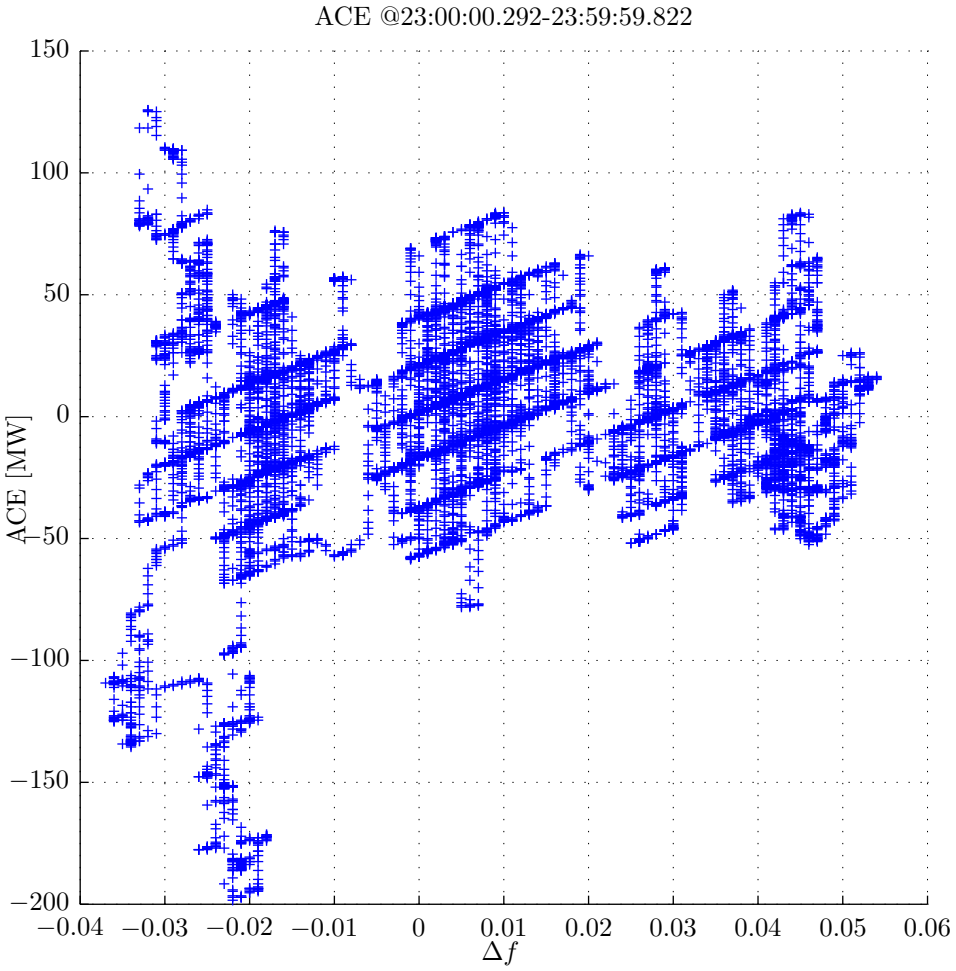

Figure 6.13: ACE as a function of Δf over one hour.

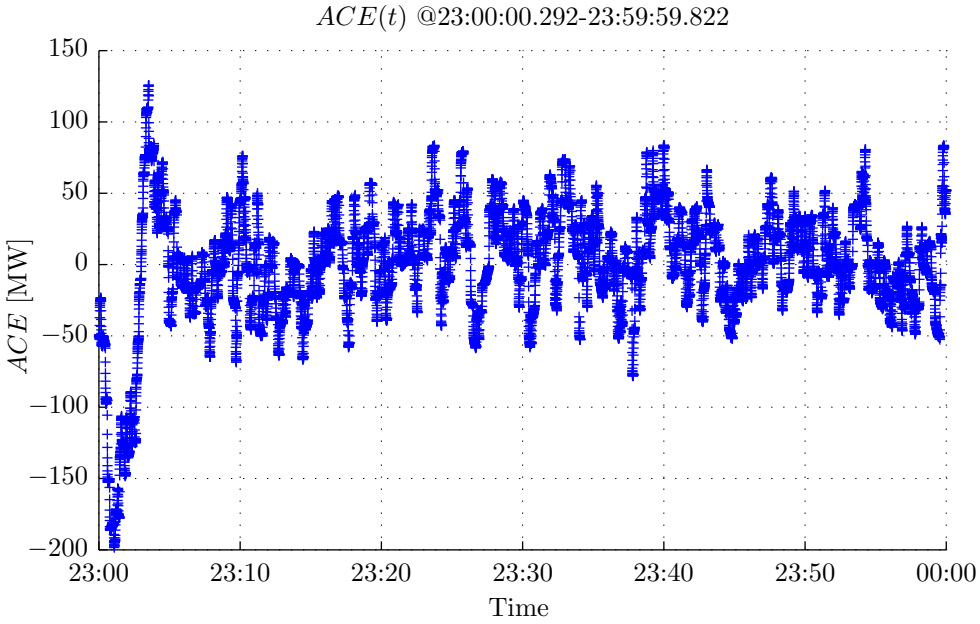

Figure 6.14: ACE as a Function of Time over One Hour.

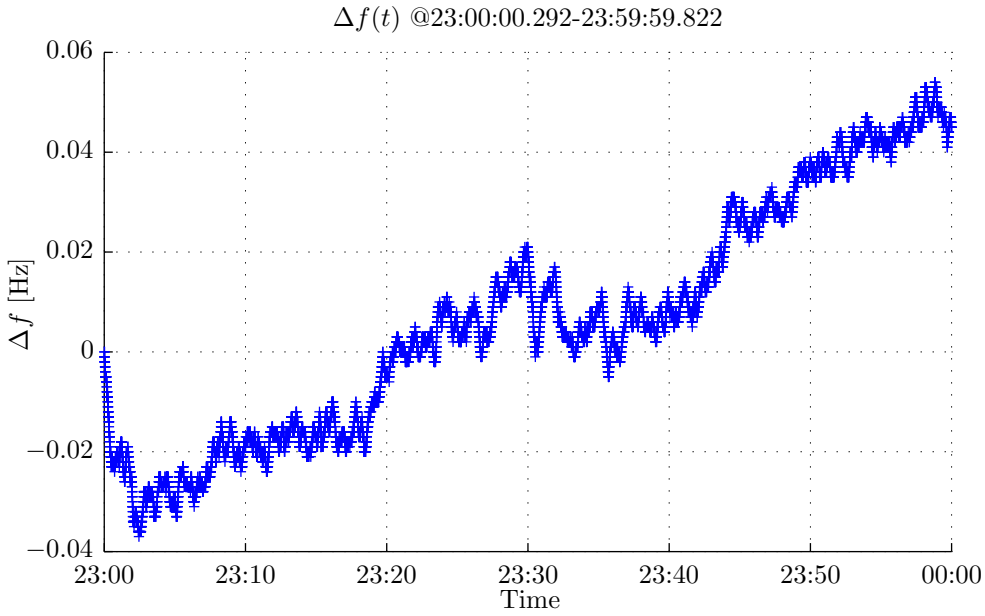

Figure 6.15: Δf as a Function of Time over One Hour.

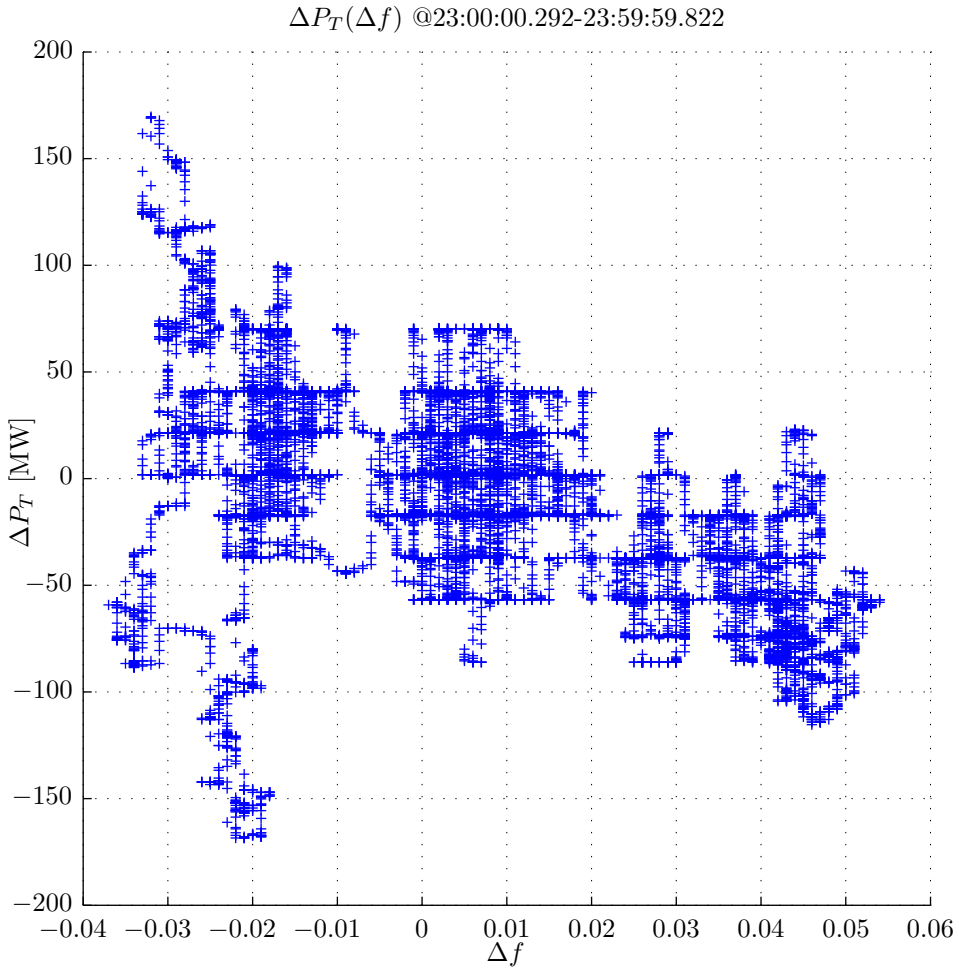

Figure 6.16: $\Delta P_{T,i}$ as a Function of Δf over One Hour.

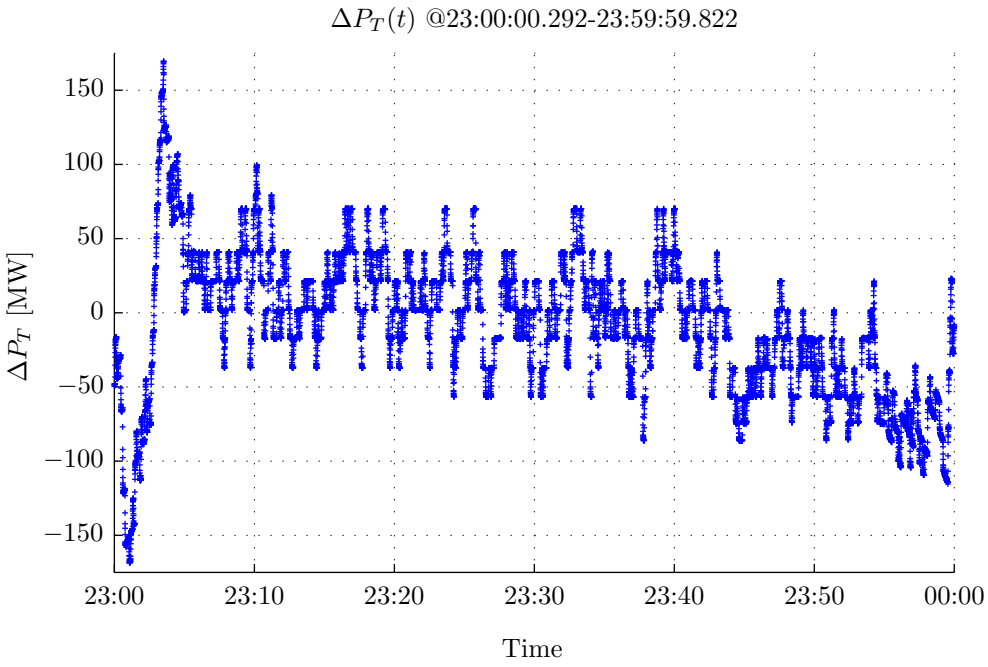

Figure 6.17: $\Delta P_{T,i}$ as a Function of Time over One Hour.

The conclusion of this analysis of the data supplied by swissgrid is that β_i can not easily be obtained by representing the tie-line powerflow as a function of the frequency deviation. As with the measurements taken during large disturbances, analyzed in section 6.4.1, it is possible that this conclusions is drawn based on errorneous data. In addition, small disturbances occur stochastically and could therefore underly statistical problems which are not treated further in the scope of this project.

Chapter 7

Discussion and Conclusion

7.1 Results from the Simulation

Due to the unforeseen difficulties encountered when determining β_i for a specific set of circumstances, the proposed improvements over the OpHB algorithm for sizing K_i could not be evaluated using the developed simulation.
If methods other than the two explained in section 6.4 for finding β_i are derived, the simulation can immediately be used to evaluate the different algorithms as explained in section 6.3.
To develop an algorithm which does not require a measured β_i for the comparison is conceivable, but a synthetic β_i will lead to a considerable loss in accuracy and comparability.
An entirely different approach to evaluating the performance of the K_i sizing algorithms is to use the backup AGC, which is present and connected to the network at all times but does not send signals to the generators, to determine the usefulness of the different K_i factors in terms of minizing ACE.

7.2 Further Research

Over the course of this project, a number of interesting topics of for future research activities in different areas were found.

Investigation of $ACE(\Delta f)$ and $\Delta P_{T,i}(\Delta f)$ to find the origins of the artifacts presented in 6.4.

Performing thorough mathematical analysis of $\Delta P_{T,i}$ for non-ideal cases, such as tie-line power flows which are not accompanied by frequency deviations or load swings.

Improving the accuracy of the simulation by implementing more dynamic phenomena such as turbine characteristics. Integrating voltage

magnitudes and angles in order to perform sophisticated power flow calculations after outages.

Researching load self-regulation in Switzerland in order to find out if the research published in [29] applies to other areas as well.

Researching surplus generation and additional Primary Control in Switzerland to improve on the standard OpHB values.

Analyzing more measurements of outages in Europe to find realistic values for β_i and to subsequently compare the different K_i factor algorithms.

Analyzing random frequency variations using stochastic mathematics and machine learning algorithms so that β_i can be "learned".

Studying the adequacy of frequency control reserves for the case of perfect AGC of all areas.

Developing a trading model for Secondary Control power in order to be able to use features of specific areas, i.a. fast response times, large reserves.

Analyzing implications of switching off Secondary Control in Switzerland.

7.3 Conclusion

The extensive literature review, as well as the analysis of the current and past frequency control regulations of the RGCE have shown considerable potential for improving the sizing of K_i, bringing it closer to β_i. Four different methods developed for this task have been outlined and integrated into a newly developed simulation program. The data delivered by swissgrid, however, was not as applicable to the simulation environment as would be desirable. Further analysis of said data revealed potentially fundamental flaws in its acquisition or in the functioning of the Swiss transmission grid. A multitude of future research directions have been elucidated, for which this report serves as a viable basis.

Appendix A

Evaluation Results

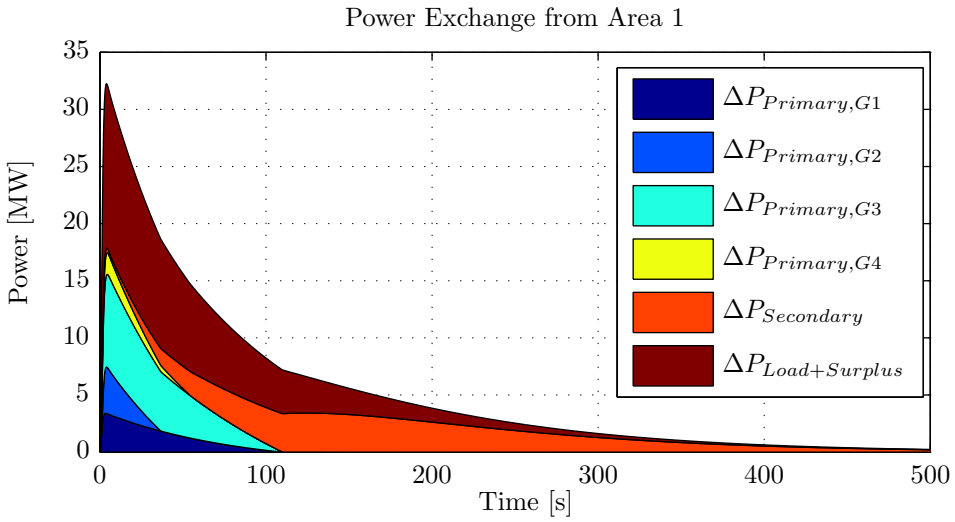

Figure A.1: Development of the Primary and Secondary Control Power, the Load Self-Regulation and the Total Power Transported over the Tie-Line over Time.

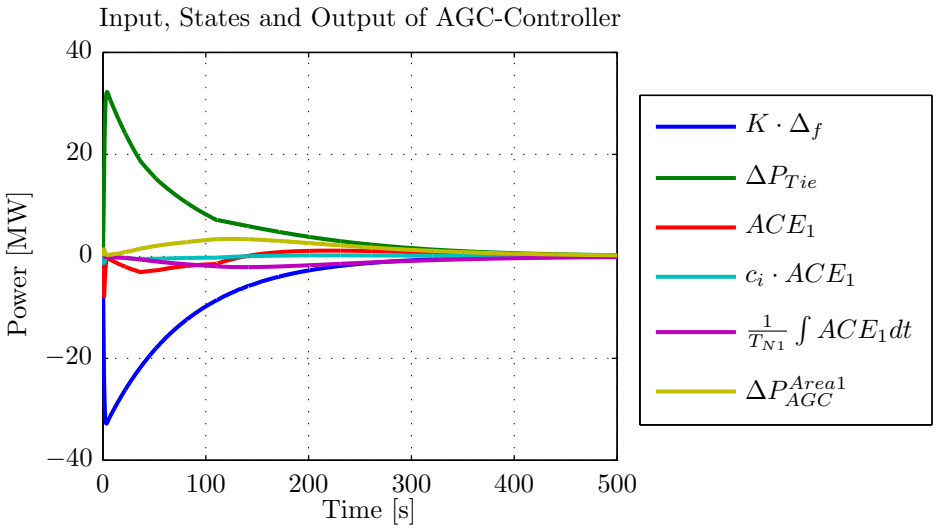

Figure A.2: Development of the AGC Inputs ($K\Delta f$, ΔP_{Tie}), Internal Variables (ACE_1, $c_i ACE_1$, $\frac{1}{T_{N,1}} \int ACE_1 dt$) as well as its Output (ΔP_{AGC}^{Area1}).

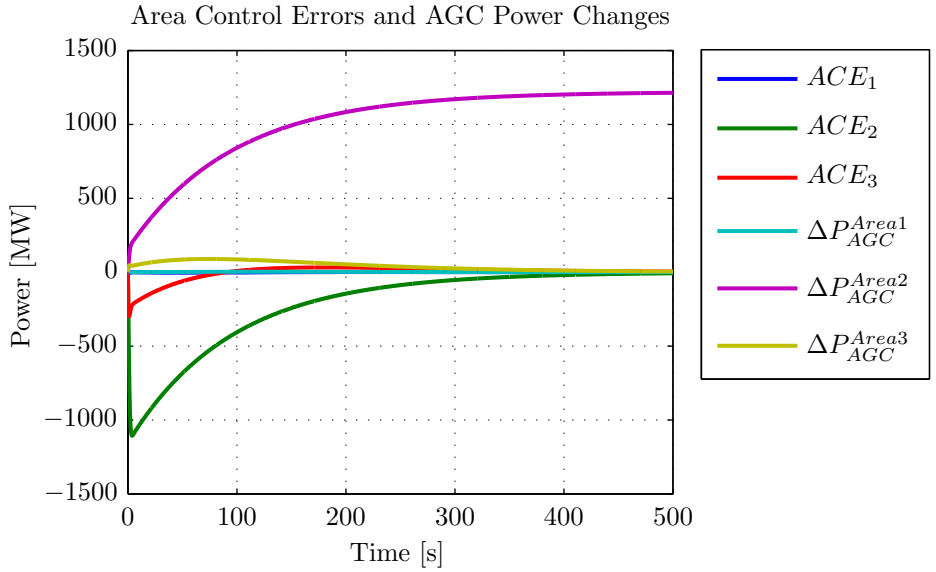

Figure A.3: Reaction of All Areas' AGC to the Disturbance in Area Two.

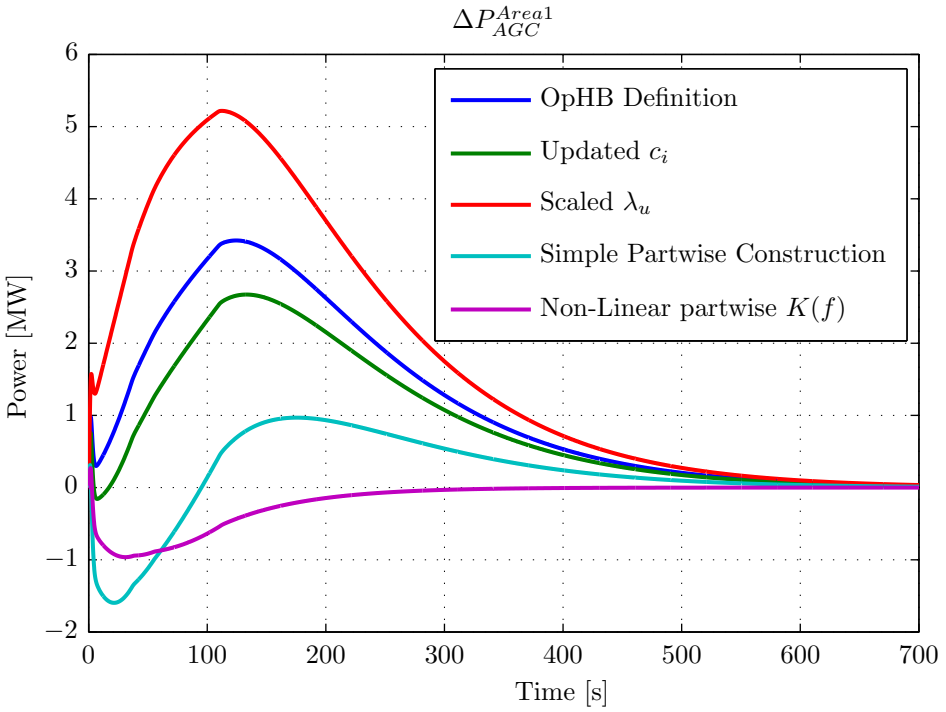

Figure A.4: Output of the First Area's AGC for the Different K_i Calculation Algorithms, which Controls the Secondary Control Power Plants.

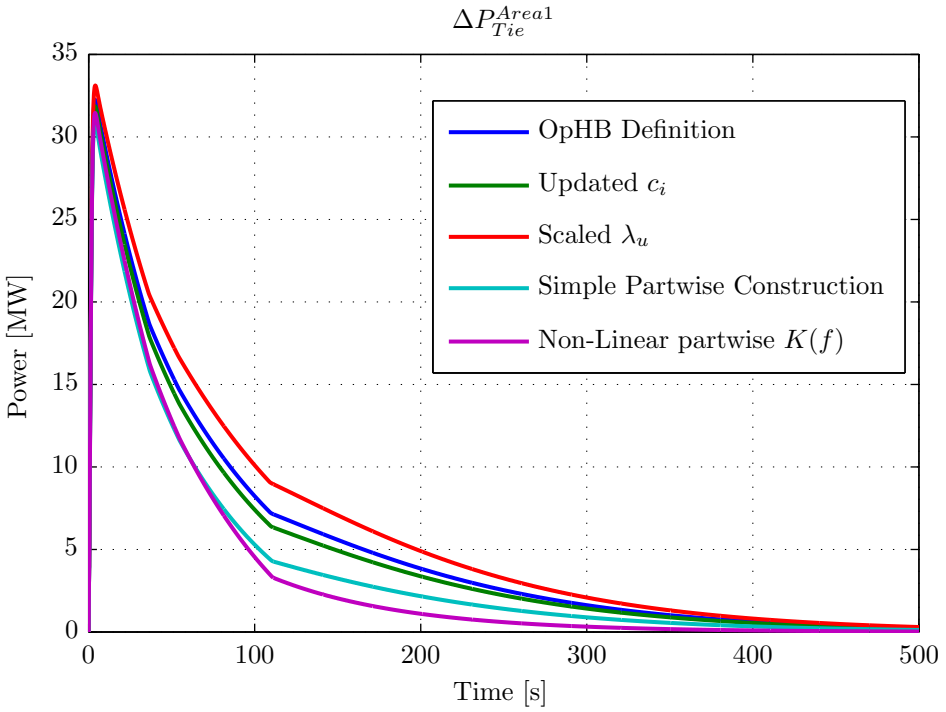

Figure A.5: Tie-line Powerflows out of Area One for the Different K_i Calculation Algorithms.

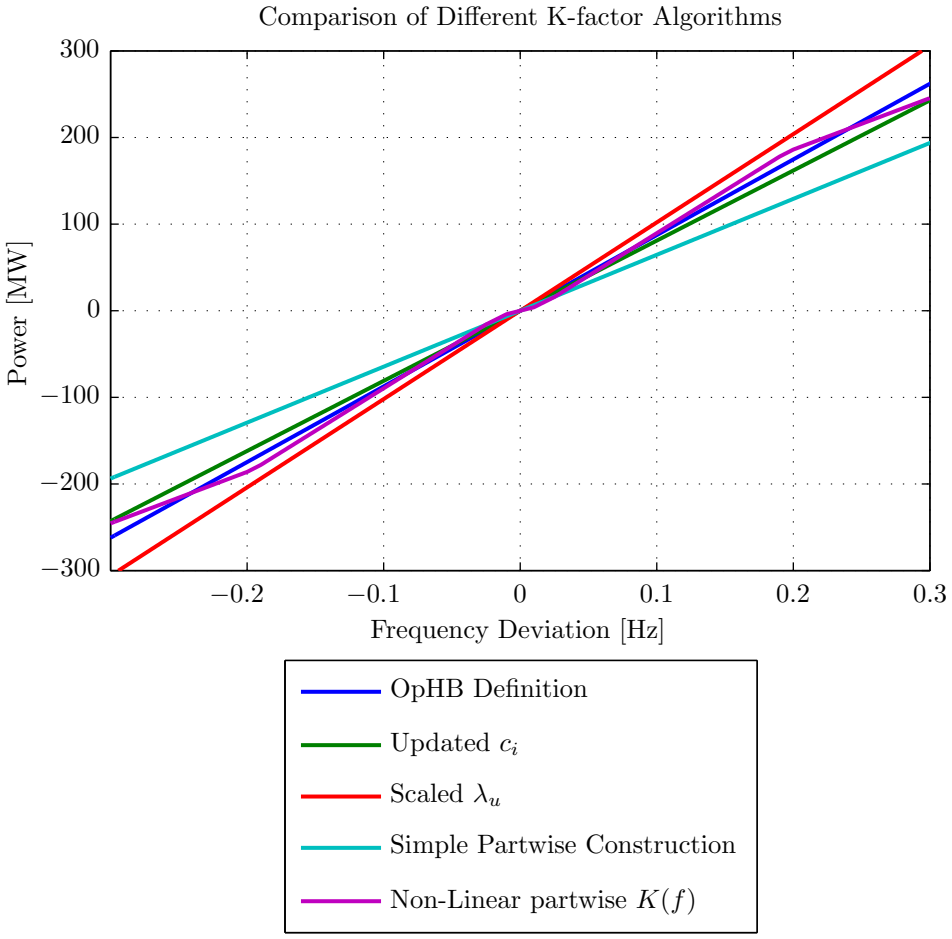

Figure A.6: Frequency Bias Factors $K_i(f)$ Resulting from the Different Algorithms.

Acronyms

ENTSO-E	European Network of Transmission System Operators for Electricity
RGCE	Regional Group Continental Europe
UCTE	Union for the Co-ordination of Transmission of Electricity
UCPTE	Union for the Coordination of Production and Transmission of Electricity
OpHB	Operation Handbook
AGC	Automatic Generation Control
LFC	Load Frequency Control
ACE	Area Control Error
CENTREL	Former synchronous area covering Czech Republic, Hungary, Poland and Slovakia
NERC	North American Electric Reliability Corporation
TSO	Transmission System Operator
EEX	European Energy Exchange

List of Figures

List of Tables

Bibliography

[1] P. Kundur, N.J. Balu, and M.G. Lauby. *Power system stability and control*, volume 19. McGraw-Hill New York, 1994.

[2] G. Andersson. *Dynamics and Control of Electric Power Systems*. EEH - Power Systems Laboratory, February 2010.

[3] UCTE OpHB-Team. *UCTE Operation Handbook Policy 1: Load-Frequency Control and Performance*. UCTE, March 2009.

[4] UCTE OpHB-Team. *UCTE Operation Handbook Appendix 1: Load-Frequency Control and Performance*. UCTE, July 2004.

[5] ENTSO-E. ENTSO-E Statistical Yearbook 2009, 2009.

[6] swissgrid ag. Grundlagen Systemdienstleisungsprodukte, Version 6.0, 2010.

[7] M. Thoma and P. Niggli. Systemdienstleistungen: Ein funktionierender Wettbewerb als Grundlage. *swissgrid.ch*, ((Version 1.6)), December 2009.

[8] N. Jaleeli, L.S. VanSlyck, D.N. Ewart, L.H. Fink, and A.G. Hoffmann. Understanding automatic generation control. *Power Systems, IEEE Transactions on*, 7(3):1106 –1122, August 1992.

[9] UCTE OpHB-Team. *UCTE Operation Handbook Policy 1: Load-Frequency Control and Performance*. UCTE, July 2004.

[10] Ibraheem, P. Kumar, and D.P. Kothari. Recent philosophies of automatic generation control strategies in power systems. *Power Systems, IEEE Transactions on*, 20(1):346 – 357, 2005.

[11] G. Quazza. Noninteracting Controls of Interconnected Electric Power Systems. *Power Apparatus and Systems, IEEE Transactions on*, PAS-85(7):727 –741, 1966.

[12] O.I. Elgerd and C.E. Fosha. Optimum Megawatt-Frequency Control of Multiarea Electric Energy Systems. *Power Apparatus and Systems, IEEE Transactions on*, PAS-89(4):556 –563, 1970.

[13] N. Cohn. Techniques for Improving the Control of Bulk Power Transfers on Interconnected Systems. *Power Apparatus and Systems, IEEE Transactions on*, PAS-90(6):2409 –2419, 1971.

[14] T. Kennedy, S.M. Hoyt, and C.F. Abell. Variable, nonlinear tie-line frequency bias for interconnected systems control. *Power Systems, IEEE Transactions on*, 3(3):1244 –1253, August 1988.

[15] L.-R. Chang-Chien, Naeb-Boon Hoonchareon, Chee-Mun Ong, and R.A. Kramer. Estimation of beta; for adaptive frequency bias setting in load frequency control. *Power Systems, IEEE Transactions on*, 18(2):904 – 911, May 2003.

[16] Le-Ren Chang-Chien and Jun-Sheng Cheng. The Online Estimate of System Parameters For Adaptive Tuning on Automatic Generation Control. In *Intelligent Systems Applications to Power Systems, 2007. ISAP 2007. International Conference on*, pages 1 –6, 2007.

[17] Branko Stojkovic. An original approach for load-frequency control– the winning solution in the Second UCTE Synchronous Zone. *Electric Power Systems Research*, 69(1):59 – 68, 2004.

[18] G.A. Chown and B. Wigdorowitz. A methodology for the redesign of frequency control for AC networks. *Power Systems, IEEE Transactions on*, 19(3):1546 – 1554, 2004.

[19] G.A. Chown and R.C. Hartman. Design and experience with a fuzzy logic controller for automatic generation control (AGC). *Power Systems, IEEE Transactions on*, 13(3):965 –970, August 1998.

[20] M. Yao, R.R. Shoults, and R. Kelm. AGC logic based on NERC's new Control Performance Standard and Disturbance Control Standard. *Power Systems, IEEE Transactions on*, 15(2):852 –857, May 2000.

[21] N. Jaleeli, L.S. VanSlyck, M.M. Yao, R.R. Shoults, and R. Kelm. Discussion of "AGC logic based on NERCs new control performance standard and disturbance control standard"; [and reply]. *Power Systems, IEEE Transactions on*, 15(4):1455 –1456, November 2000.

[22] Rapport Annuel UCPTE, 1957 - 1958. Heidelberg, DE; 1958.

[23] Rapport Annuel UCPTE, 1958 - 1959. Heidelberg, DE; 1959.

[24] Rapport Annuel UCPTE, 1990. Arnhem, NL; Aug. 1991.

[25] Rapport Annuel UCPTE, 1981 - 1982. Rhode-St.-Genèse, BE; Nov. 1982.

[26] H. Weber, B. Madsen, H. Asal, and E. Grebe. Kennzahlen der Primärregelung im UCPTE-Netz und künftige Anforderungen. *Elektrizitätswirtschaft*, Magazine 4, Jg. 96:p. 132–137, 1997.

[27] C. Concordia. Effect of Prime-Mover Speed Control Characteristics on Electric Power System Performance. *Power Apparatus and Systems, IEEE Transactions on*, PAS-88(5):752 –756, May 1969.

[28] C. Concordia, L. K. Kirchmayer, and E. A. Szymanski. Efect of Speed-Governor Dead Band on Tie-Line Power and Frequency Control Performance. *Power Apparatus and Systems, Part III. Transactions of the American Institute of Electrical Engineers*, 76(3):429 –434, 1957.

[29] E. Welfonder, B. Hall, W. Glaunsinger, and R. Heueck. Untersuchung der frequenz- und spannungsabhängigen Leistungsaufnahmen von Verbraucherteilnetzen - Ergebnisse und Folgerungen für den Verbundbetrieb. *Elektrizitätswirtschaft Jg. 93 (1994), Heft 3*, 1994.

[30] W. Glaunsinger, R. Heueck, E. Welfonder, and B. Hall. Study of the Dependence of Consumer Subsystems on Frequency and Voltage. In *Cigré 1994 Session, Ref. 39/11-04*, 1994.

[31] Nathan Cohn. Decomposition of Time Deviation and Inadvertent Interchange on Interconnected Systems, Part I: Identification, Separation and Measurement of Components. *Power Engineering Review, IEEE*, PER-2(5):37, May 1982.

[32] M. Scherer, D. Schlipf, and W. Sattinger. Test zur Primärregelfähigkeit, April 2011. Version 1.0.

[33] ENTSO-E Data Portal. Website: https://www.entsoe.eu/resources/data-portal/. Database from 17.4.2011.

[34] J. Carpentier. 'To be or not to be modern' that is the question for automatic generation control (point of view of a utility engineer). *International Journal of Electrical Power & Energy Systems*, 7(2):81 – 91, 1985.

[35] H. Glavitsch and J. Stoffel. Automatic generation control. *International Journal of Electrical Power & Energy Systems*, 2(1):21 – 28, 1980.

[36] Y. G. Rebours, D. S. Kirschen, M. Trotignon, and S. Rossignol. A Survey of Frequency and Voltage Control Ancillary Services - Part I: Technical Features. *Power Systems, IEEE Transactions on*, 22(1):350 –357, 2007.

[37] L.S. VanSlyck, N. Jaleeli, and W.R. Kelley. A comprehensive shakedown of an automatic generation control process. *Power Systems, IEEE Transactions on*, 4(2):771 –781, May 1989.

[38] Louis S. VanSlyck, Nasser Jaleeli, and W. Robert Kelley. Implications of Frequency Control Bias Settings on Interconnected System Operation and Inadvertent Energy Accounting. *Power Engineering Review, IEEE*, 9(5):69, May 1989.